UC Berkeley
UC Berkeley Electronic Theses and Dissertations

Title
The Circuit Mechanisms Underlying the Spatiotemporal Properties of Stage 1 Retinal Waves

Permalink
https://escholarship.org/uc/item/206370pn

Author
Voufo, Christiane W

Publication Date
2022

Peer reviewed|Thesis/dissertation

eScholarship.org Powered by the California Digital Library
University of California

The Circuit Mechanisms Underlying the Spatiotemporal Properties of Stage 1 Retinal Waves

By

Christiane W. Voufo

A dissertation submitted in partial satisfaction of the

requirements for the degree of

Doctor in Philosophy

in

Neuroscience

in the

Graduate Division

of the

University of California, Berkeley

Committee in charge:

Professor Marla B. Feller, Chair
Professor Helen Bateup
Professor Teresa Puthussery
Professor Gian Garriga

Fall 2022

The Circuit Mechanisms Underlying the Spatiotemporal Properties of Stage 1 Retinal Waves

Copyright 2022
by
Christiane W. Voufo

Abstract

The Role of Acetylcholine and Gap Junctions in the Generation of Stage 1 Retinal Waves

By

Christiane W. Voufo

Doctor of Philosophy in Neuroscience

University of California, Berkeley

Professor Marla Feller, Chair

Spontaneous activity is a hallmark of developing neural systems. In the developing visual system, patterned spontaneous activity begins in the retina, where waves of depolarizations, called retinal waves propagate across a network of neurons. Retinal waves propagate laterally across the retina, but also downstream in the visual circuit through the dorsal lateral geniculate nucleus, the superior colliculus (SC), and the primary visual cortex. Throughout the development of the mouse visual system, retinal waves are observed in three stages starting from embryonic day 16 (E16) to eye opening, corresponding to postnatal day 13 (P13). The circuits that mediate each stage of retinal waves change throughout development. Stage 2 waves are observed between P1-P10 and are initiated by the release of acetylcholine (ACh) from starburst amacrine cells (SACs), leading to the activation of nicotinic acetylcholine receptors (nAChRs). They propagate through a network of SACs that themselves express nAChRs during development. Stage 3 waves are observed between P10-P14 and are initiated by the release of glutamate from bipolar cells, leading to the activation of ionotropic glutamate receptors. Stage 3 waves propagate through a network of bipolar and amacrine cells via glutamate transmission and gap junction coupling. Stage 1 waves are observed between E16-P0 and the initiation and propagation mechanisms for Stage 1 waves have been thought to mainly rely on gap junction coupling between retinal ganglion cells (RGCs), unlike the other two stages the details of their initiation and propagation mechanisms are poorly understood.

The focus of this dissertation is to describe the spatiotemporal properties and circuit mechanisms of Stage 1 waves, identify how distinct these waves are from Stage 2 waves, and then begin to probe their function in the development of the retina. In Chapter 1, I summarize the current understanding of the mechanisms shaping the spatiotemporal properties of all stages of retinal waves. In Chapter 2, I used a custom-built macroscope and a two-photon microscope to perform population calcium imaging in embryonic retinas. I first characterized the spatiotemporal properties of Stage 1 waves. Then, using genetic and pharmacological manipulations, I determined the relative role of gap junctions and nAChRs in mediating Stage 1 waves. Stage 1 waves initiate at several locations across the retina and propagate across finite regions of varying areas. Additionally, I found that waves that spanned a large retinal surface area were more sensitive to nAChRs and gap junction antagonists, as they were either abolished or significantly

reduced in frequency in the presence of those pharmacological agents. I also found that waves in mice lacking the β2 subunit of nAChRs (β2-nAChR-KO) exhibited reduced propagation areas. The application of a general nAChR antagonist in the β2-nAChR-KO had no effect on wave properties. However, the application of a gap junction antagonist greatly reduced both the area and frequency of waves, suggesting a compensatory role for gap junctions in the β2-nAChR-KO.

The disruption of Stage 1 and 2 waves in the β2-nAChR-KO allowed for further investigation into the role of retinal waves in regulating the maturation of RGCs. We specifically investigated a subpopulation of RGCs, called intrinsically photosensitive RGCs (ipRGCs). Using immunohistochemistry, we observed a significant reduction in ipRGC density between P1 and P7 retinas in both WT and β2-nAChR-KO mice, suggesting that ipRGC cell death observed in the first postnatal week of development occurs independently of normal retinal waves. Moreover, there was no significant change in density or spatial distribution between WT and β2-nAChR-KO mice at P1 and P7, also indicating this developmental step occurs independently of normal waves. In Chapter 3, I discuss the implications of these results on our current understanding of retinal waves. Specifically, I highlight newly found key similarities and differences between Stage 1 and 2 waves, and future experiments necessary to fully understand the distinction between them.

To
My parents Alfred and Mireille Voufo
Thank you for teaching me the importance of hard work

Table of Contents

List of Figures

List of Tables

ACKNOWLEDGMENTS

Getting a PhD in neuroscience is not an easy task. Being the first in your family to get a PhD is a whole other beast. There were many firsts for me on this journey. Although I had to face many on my own, there were many more I did not have to face alone. The community I was able to find and build during my PhD provided me with the motivation and support I needed to accomplish this monumental goal.

Marla, you have been instrumental to my growth and success as a scientist. From the moment we met, you have provided space for me to speak openly, even though I was a little scared to do so at times. Your humility and confidence as a scientist inspired me every day. I've been blessed to have you as my mentor.

Helen, Teresa and Gian, I am also grateful to all of you for your kind delivery of constructive feedback. You all have helped me to think more critically about my work and also helped to create a safe space for me to express myself. I am especially grateful for your continued understanding and judgement free interactions with me.

The Feller lab has been an interesting place to do my thesis work in. I have met so many different personalities over the years all of whom have helped me learn something in one form or another. The current and past members of the lab are all incredible scientists and their excellence definitely helped to provide fuel for my fire whenever it was close to burning out. I'm glad that I got the chance to interact with Franklin, Mathew, Corey, Malak, Ryan, Kimberley, Paley, Anna, Josh, Karina, Miah, Samira, Rachana, Rongshan, Kaylin, Remy, Jocelyn, Noah and all the rotation students we've had.

Alex, you are one of the kindest humans I've come across. During the height of the pandemic your guidance and support with data analysis really helped my thesis gain some much-needed momentum. I have learned so much from you and these lessons I will carry with me for as long as I can remember them. Thank you for your mentorship and friendship.

Dariya, Michelle, Madeline and Amanda, you have been great friends over the years, and I am looking forward to seeing where life takes us. Dariya, you give the best advice ever! I'm grateful for our many coffee dates, attempted book clubs, study sessions, and general hangouts. You are such a treasure of a friend. I'm glad we have been able to be there for each other.

Gift and Ntemena, you ladies have been the home away from home I so desperately needed. I thank God for bringing us together. I'm grateful for the laughter we shared and the life we have lived together thus far. Thank you for bringing joy, warmth, and love into my apartments! Love you both very dearly. Special thanks to Madam Ntemena for being a true VIP, you never fail to show up for your friends when they need you most and for that I am grateful.

To my beautiful and very loud family, thank you for keeping me humble. Thank you for being my reason to push.

“Beyond the question of what you push through is what you push for”

- Stacey Abrams

Chapter 1

Introduction to Retinal Waves

The mammalian retina is a thin structure at the back of the eye that turns light from our environment into electrical signals that our brains can understand (Azeredo da Silveira & Roska, 2011). Although small, the retina is a well-organized structure composed of five-layers. Three of those layers are cellular, with light-sensing neurons called photoreceptors in its outermost layer, interneurons in its middle layer and projection neurons called RGCs in its inner most layer (closest to the lens). The other two layers are referred to as plexiforms, as they house the synaptic plexus connecting photoreceptors to interneurons and interneurons to RGCs. The synapses between neurons of the retina form microcircuits that solve multiple computational problems, allowing the retina to process information like color, contrast, luminance, motion, and direction in addition to the presence/absence of light (Azeredo da Silveira & Roska, 2011; Summers, El Quessney, & Feller, 2021; Dhande et al., 2015). This information is relayed to specific brain regions that further process this information, enabling the perception of object location, distance, etc. The precise targeting of RGCs to these brain regions occurs in an activity independent manner during development, where the presence of spontaneous activity originating from the retina, called retinal waves, is important for the refinement of RGC axons into finite termination zones within these target regions. Over the past two decades, a growing body of work on retinal waves has allowed us to characterize, model and determine the cellular mechanisms in the retina that generates them. Yet there is still more to uncover, especially understanding the role they play in the development of retinal circuitry. Here, I will briefly summarize our current understanding of retinal waves.

The circuits that mediate retinal waves change with development and have been classified into three stages

Early in its development, the retina is subject to periods of spontaneous activity. This activity comes in the form of propagating depolarizations called retinal waves. Retinal waves persist during an extended period of development. In mice, this period starts a few days prior to birth until 2 weeks after birth, when mice open their eyes. During this time, the retina itself is undergoing a tremendous amount of development. As the retina develops, the circuits that mediate waves also change, which in turn changes the spatiotemporal properties of waves (Maccione et al., 2014). These circuit mechanisms have been divided into 3 stages, retinal waves present in postnatal retinas (Stage 2 and 3 waves) are the most well understood. They employ two different initiation and propagation mechanisms, with waves present during the first postnatal week (Stage 2) using a cholinergic circuit and those present during the second postnatal week (Stage 3) using a glutamatergic circuit.

Stage 2 waves

The mechanism underlying the initiation and propagation of Stage 2 waves have been extensively studied. Stage 2 waves are observed during the first postnatal week of development, between P1 and P8. These waves were the first recorded in the prenatal rat retina (Maffei & Galli-Resta, 1990) and then in the postnatal ferret retina (Meister et al., 1991). Using a multielectrode array (MEA), it was found that this correlated spontaneous activity presented as action potentials that propagated across the RGC layer in a wave-like manner (Meister et al., 1991). Later work showed that Stage 2 waves had a distinct set of spatiotemporal properties. One such property was the refractory period of the waves, which referred to the minimum interval of time (approximately 1 min) during which an area of retina recently activated by a wave cannot participate in another (Feller et al., 1997). This refractory period also set the grounds for another spatiotemporal property called domain/wave size, which was set by strict boundaries that distinguished areas of the retina in refraction from those that were not (Feller et al., 1997). Given the distribution of wave size and inter-wave-interval, a computational model called the two-layer model was deduced. In this model, Stage 2 waves are initiated, propagated, and terminated by a layer comprised of a network of acetylcholine releasing interneurons called starburst amacrine cells (SACs). This activation would subsequently be read-out by a layer of neighboring RGCs as a retinal wave, which provides a spatial and temporal filter of the activity in the SAC layer. This model was based on previous work demonstrating that cholinergic signaling between SACs and RGCs was important for this read-out of waves to occur, but the nature of the connection between SACs remained to be determined (Feller et al., 1996).

Following the description of the two-layer model, other computational models were described to explain the spatiotemporal properties of Stage 2 waves. What they all had in common was the incorporation of a Gaussian distribution of refractory periods in SACs (Godfrey & Eglen, 2009). Between these models, several predictions were made explaining how SAC physiology set the spatiotemporal properties of Stage 2 waves: (1) waves are initiated by the spontaneous depolarization of single SACs, (2) waves propagated via a cholinergic network between neighboring SACs, (3) wave boundaries are determined by a slow afterhyperpolarization (sAHP) in clusters of nearby SACs that provided a refractory period temporarily preventing propagation of subsequent waves and (4) the varying wave sizes are determined by the interplay between infrequent spontaneous depolarization of SACs (Ford et al., 2012). Several of these assumptions were later confirmed by experimental observations. Using, electrophysiology, two-photon calcium imaging, pharmacology, cell-based neurotransmitter fluorescent engineered reporter (CNiFERs) imaging and modeling, it was shown that the Stage 2 wave initiation was indeed dependent on the spontaneous depolarization of SACs and its propagation was set by the recurring cholinergic network between neighboring SACs (Ford et al., 2012). Additionally, it was also shown that the sAHP of SACs was important for setting up the refractory period of SACs and that the magnitude of a SACs depolarization was directly proportional to the duration of its sAHP (Ford et al., 2012).

Stage 3 waves

Like Stage 2 waves, the mechanism underlying the initiation and propagation of Stage 3 waves have been extensively studied. Stage 3 waves are observed during the second postnatal week of development, between P10 and P13. The spatiotemporal properties of Stage 3 waves are very different from those observed in Stage 2 waves, suggesting the presence of different initiation and propagation mechanisms. Unlike Stage 2 waves that occur only once per minute per unit area of the retina, Stage 3 waves occur in clusters of 2-5 waves initiated in quick succession of each other in the same location on the retina with 1-2 minutes between these bouts of activity (Blankenship & Feller, 2010).

Stage 3 retinal waves are mediated by glutamate release from bipolar cells (Akrouh & Kerschensteiner, 2013; Blankenship et al., 2009; Wong, 1999). Using voltage clamp recordings from RGCs Blankenship revealed that during Stage 3 waves, RGCs receive excitatory synaptic inputs that are blocked after the application of AMPA/Kainate and NMDA receptor antagonists (Blankenship et al., 2009). The source of glutamate received by RGCs in the retina comes from either VGLUT3 expressing amacrine cells or VGLUT1 expressing bipolar cells. Voltage clamp recordings of RGCs in knockouts (KOs) for VGLUT1 and VGLUT3 revealed that glutamate release from bipolar cells was the main source of the glutamate that mediated Stage 3 waves (Blankenship et al., 2009). Furthermore outside-out patch recordings on RGCs showed that most wave associated currents were accompanied by glutamate currents, suggesting that glutamate release occurs as a spillover (Blankenship et al., 2009). Additionally, enhancing this spillover by either blocking excitatory amino acid transporters or inhibition increased the number of bursts observed (Blankenship et al., 2009). These results suggest that glutamate spillover is important for setting up the bursting behavior of Stage 3 waves. This was confirmed by subsequent studies using glutamate sensors (Firl et al., 2013; Rosa et al., 2015; Bos et al., 2016)

Glutamate mediated excitation is not the only regulator of Stage 3 waves' spatiotemporal properties. GABA and glycine mediated inhibition has also been shown to be involved. The source of GABA and glycine in the retina comes from amacrine cells that are either GABAergic (63 different types) or glycinergic (13 different types) (Yan et al., 2020). Blocking GABAergic and glycinergic signaling with $GABA_A$ and glycine receptor antagonists increased the frequency of bursts, as was observed after the blockage of glutamate signaling (Blankenship et al., 2009; Akrouh & Kerschensteiner, 2013). Additionally, gap junction coupling between ON cone bipolar cells has been implicated in the generation of Stage 3 waves (Akrouh & Kerschensteiner, 2013).

The spontaneous release of glutamate from bipolar cells has been viewed as the mechanism for the initiation of Stage 3 waves, but more recent work has shown that light stimulation can initiate them as well. Stage 3 waves occur during a time in retinal development where the outer retina gets synaptically connected to the inner retina, which occurs between P10-P14 (Tian & Copenhagen, 2003). The development of this synaptic connection allows the stimulation of photoreceptors to drive wave initiation. Waves were initiated by both the onset and offset of

light, indicating that both the ON and OFF pathways are involved in this wave initiation mechanism (Tiriac et al., 2018). Although light initiates waves, the duration of the light stimulus had an inverse relationship to wave frequency, where constant light decreased frequency and short pulses of light increased frequency (Tiriac et al., 2018). Additionally, waves were initiated at the same location of light stimulus presentation (Tiriac et al., 2018).

Stage 1 waves

Though much is known about the circuit mechanisms generating waves after birth, very little is known about the wave generating mechanism during embryonic development. In mice, Stage 1 waves are observed between E16 and P0 (Bansal et al., 2000) while in rabbit they are present at E22 (Syed et al., 2004). In rabbit, Stage 1 waves persist in the presence of pharmacological antagonists of ionotropic neurotransmitter receptors and are blocked by gap junction antagonists (Syed et al., 2004). In mice, Stage 1 waves consist of large propagating waves and small non-propagating events (Bansal et al., 2000). The application of nAChR antagonists inhibits larger propagating events (Bansal et al., 2000). Though there is no anatomical evidence of synapses as early as E16-18, recent work has shown that SACs are present embryonically, begin to migrate to the inner nuclear layer (INL), and send projections to the inner plexiform layer (IPL) guided by homotypic contacts (Ray et al., 2018). Hence cholinergic signaling is likely occurring via the volumetric release of ACh. Exactly how gap junctions and cholinergic signaling set the spatiotemporal properties of Stage 1 waves remains to be understood. One of the goals of my thesis is to describe the spatiotemporal properties of Stage 1 waves and determine how similar they are to those of Stage 2 waves.

Interactions between Stage 1 waves and intrinsically photosensitive retinal ganglion cells

Before the development and maturation of traditional photoreceptors, the retina is dependent on a nontraditional type of photoreceptors for light detection, called intrinsically photosensitive retinal ganglion cells (ipRGCs). There are multiple types of ipRGCs that have very diverse morphology, physiology, and projection patterns. ipRGCs mediate various light induced behaviors during development such as, light aversion and time-restricted feeding (Caval-Holme & Feller, 2019; Fernandez et al., 2020). As the first light sensitive cells in the retina to be born, their intrinsic photosensitivity plays a role in mediating and modulating several key developmental processes in the retina that include, but are not limited to regression of the hyaloid, a transient vascularization that precedes adult vascularization, ocular growth, and retinal wave plasticity, a term used to describe compensatory activity that appears in mouse models that lack Stage 2 retinal waves (Lucas & Schmidt, 2019; Rao et al., 2013; Liu et al., 2022; Kirkby & Feller, 2013; Arroyo et al., 2016; Caval-Holme et al., 2022). Concurrent with the onset of Stage 1 waves is the completion of ipRGC proliferation (Lucas and Schmidt, 2019; McNeill et al., 2011) and differentiation (Shekhar et al., 2022; Whitney et al., 2022). ipRGCs also undergo a period of cell death during the first postnatal week of development, which has been shown to regulate ipRGC mosaic formation as well as rod and cone mediated circadian photoentrainment (Chen et al., 2013).

The work done on the functional relevance of spontaneous activity in the retina has focused on its effects on retinal projections. Stage 2 and Stage 3 waves have been shown to be important for the eye-specific segregation of retinal projections to the dorsal lateral geniculate nucleus and retinotopic organization of retinal projections to the SC (Tiriac et al., 2018; Kirkby et al., 2013; Dhande et al., 2011; McLaughlin et al., 2003). However, not much is known on the effects this spontaneous activity plays in the development of retinal circuits.

One potential developmental phenomenon that occurs at the same times is retinal waves is cell death, 50% of retinal ganglion cells die, including 50% of ipRGCs (Farah & Easter, 2005; Bahr, 2000). In some systems, correlated network activity has been implicated in cell proliferation and cell death. For example, retinal wave activity promotes neurite outgrowth and potentially survival among RGCs (Goldberg et al., 2002). Additionally, in the developing primary somatosensory and motor cortices, higher levels of spontaneous electrical activity were shown to have a neuroprotective effect (Blanquie et al., 2017). In my thesis, I investigate the role of Stage 1 and Stage 2 retinal waves in the regulation of ipRGC death by measuring the density and spatial distribution, due to their early maturation and easily accessible targeting tools.

REFERENCES

Akrouh, A., & Kerschensteiner, D. (2013). Intersecting circuits generate precisely patterned retinal waves. *Neuron*, *79*(2), 322–334. https://doi.org/10.1016/j.neuron.2013.05.012

Arroyo, D. A., Kirkby, L. A., & Feller, M. B. (2016). Retinal Waves Modulate an Intraretinal Circuit of Intrinsically Photosensitive Retinal Ganglion Cells. *Journal of Neuroscience*, *36*(26), 6892–6905. https://doi.org/10.1523/jneurosci.0572-16.2016

Azeredo da Silveira, R., & Roska, B. (2011). Cell Types, Circuits, Computation. *Current Opinion in Neurobiology*, 664-671. https://doi.org/10.1016/j.conb.2011.05.007

Bahr, M. (2000). Live or let die - retinal ganglion cell death and survival during development and in the lesioned adult CNS. *Trends in Neurosciences*, *23*(10), 483–490. https://doi.org/10.1016/S0166-2236(00)01637-4

Bansal, A., Singer, J. H., Hwang, B. J., Xu, W., Beaudet, A., & Feller, M. B. (2000). Mice Lacking Specific Nicotinic Acetylcholine Receptor Subunits Exhibit Dramatically Altered Spontaneous Activity Patterns and Reveal a Limited Role for Retinal Waves in Forming ON and OFF Circuits in the Inner Retina. *Journal of Neuroscience*, *20*(20), 7672–7681. https://www.jneurosci.org/content/20/20/7672.long

Blankenship, A. G., & Feller, M. B. (2010). Mechanisms underlying spontaneous patterned activity in developing neural circuits. *Nature Reviews Neuroscience*, *11*(1), 18–29. https://doi.org/10.1038/nrn2759

Blanquie, O., Yang, J.-W. W., Kilb, W., Sharopov, S., Sinning, A., & Luhmann, H. J. (2017). Electrical activity controls area-specific expression of neuronal apoptosis in the mouse developing cerebral cortex. *ELife*, *6*. https://doi.org/10.7554/eLife.27696

Bos, R., Gainer, C., & Feller, M. B. (2016). Role for visual experience in the development of direction-selective circuits. *Current Biology*, *26*(10), 1367–1375. https://doi.org/10.1016/j.cub.2016.03.073

Caval-Holme, F., & Feller, M. B. (2019). Gap Junction Coupling Shapes the Encoding of Light in the Developing Retina. *Current Biology*, *29*(23), 4024-4035.e5. https://doi.org/10.1016/j.cub.2019.10.025

Caval-Holme, F., Aranda, M. L., Chen, A. Q., Tiriac, A., Zhang, Y., Smith, B., Birnbaumer, L., Schmidt, T. M., & Feller, M. B. (2022). The Retinal Basis of Light Aversion in Neonatal Mice. *The Journal of Neuroscience*, *42*(20), 4101–4115. https://doi.org/10.1523/JNEUROSCI.0151-22.2022

Chen, S. K., Chew, K. S., McNeill, D. S., Keeley, P. W., Ecker, J. L., Mao, B. Q., Pahlberg, J.,

Kim, B., Lee, S. C. S., Fox, M. A., Guido, W., Wong, K. Y., Sampath, A. P., Reese, B. E., Kuruvilla, R., & Hattar, S. (2013). Apoptosis Regulates ipRGC Spacing Necessary for Rods and Cones to Drive Circadian Photoentrainment. *Neuron*, *77*(3), 503–515. https://doi.org/10.1016/j.neuron.2012.11.028

Dhande, O. S., Hua, E. W., Guh, E., Yeh, J., Bhatt, S., Zhang, Y., Ruthazer, E. S., Feller, M. B., & Crair, M. C. (2011). Development of Single Retinofugal Axon Arbors in Normal and 2 Knock-Out Mice. *Journal of Neuroscience*, *31*(9), 3384–3399. https://doi.org/10.1523/jneurosci.4899-10.2011

Farah, M. H., & Easter, S. S. (2005). Cell birth and death in the mouse retinal ganglion cell layer. *Journal of Comparative Neurology*, *489*(1), 120–134. https://doi.org/10.1002/cne.20615

Feller, M. B., Butts, D. A., Aaron, H. L., Rokhsar, D. S., & Shatz, C. J. (1997). Dynamic processes shape spatiotemporal properties of retinal waves. *Neuron*, *19*(2), 293–306. https://doi.org/10.1016/S0896-6273(00)80940-X

Feller, M. B., Wellis, D. P., Stellwagen, D., Werblin, F. S., & Shatz, C. J. (1996). Requirement for cholinergic synaptic transmission in the propagation of spontaneous retinal waves. *Science*, *272*(5265), 1182–1187. https://doi.org/10.1126/science.272.5265.1182

Fernandez, D. C., Komal, R., Langel, J., Duy, P. Q., Penzo, A., Zhao, H., Hattar, S., & Haven, N. (2020). *Entrainment To Food*. *581*(7807), 194–198. https://doi.org/10.1038/s41586-020-2204-1.Retinal

Firl, A., Sack, G. S., Newman, Z. L., Tani, H., & Feller, M. B. (2013). Extrasynaptic glutamate and inhibitory neurotransmission modulate ganglion cell participation during glutamatergic retinal waves. *Journal of Neurophysiology*, *109*(7), 1969–1978. https://doi.org/10.1152/jn.00039.2013

Ford, K. J., Félix, A. L., & Feller, M. B. (2012). *Cellular Mechanisms Underlying Spatiotemporal Features of Cholinergic Retinal Waves*. https://doi.org/10.1523/JNEUROSCI.5309-12.2012

Godfrey, K. B., & Eglen, S. J. (2009). Theoretical models of spontaneous activity generation and propagation in the developing retina. *Molecular BioSystems*, *5*(12), 1527–1535. https://doi.org/10.1039/b907213f

Goldberg, J. L., Espinosa, J. S., Xu, Y., Davidson, N., Kovacs, G. T. A., & Barres, B. A. (2002). Retinal ganglion cells do not extend axons by default: Promotion by neurotrophic signaling and electrical activity. *Neuron*, *33*(5), 689–702. https://doi.org/10.1016/S0896-6273(02)00602-5

Kirkby, L. A., & Feller, M. B. (2013). Intrinsically photosensitive ganglion cells contribute to

plasticity in retinal wave circuits. *Proceedings of the National Academy of Sciences*, *110*(29), 12090–12095. https://doi.org/10.1073/PNAS.1222150110

Kirkby, L. A., Sack, G. S., Firl, A., & Feller, M. B. (2013). A role for correlated spontaneous activity in the assembly of neural circuits. *Neuron*, *80*(5), 1129–1144. https://doi.org/10.1016/j.neuron.2013.10.030

Liu, A. L., Liu, Y. F., Wang, G., Shao, Y. Q., Yu, C. X., Yang, Z., Zhou, Z. R., Han, X., Gong, X., Qian, K. W., Wang, L. Q., Ma, Y. Y., Zhong, Y. M., Weng, S. J., & Yang, X. L. (2022). The role of ipRGCs in ocular growth and myopia development. *Science Advances*, *8*(23). https://doi.org/10.1126/sciadv.abm9027

Lucas, J. A., & Schmidt, T. M. (2019). Cellular properties of intrinsically photosensitive retinal ganglion cells during postnatal development. *Neural Development*, *14*(1), 1–19. https://doi.org/10.1186/s13064-019-0132-2

Maccione, A., Hennig, M. H., Gandolfo, M., Muthmann, O., van Coppenhagen, J., Eglen, S. J., Berdondini, L., & Sernagor, E. (2014). Following the ontogeny of retinal waves: Pan-retinal recordings of population dynamics in the neonatal mouse. *Journal of Physiology*, *592*(7), 1545–1563. https://doi.org/10.1113/jphysiol.2013.262840

Maffei, L., & Galli-Resta, L. (1990). Correlation in the discharges of neighboring rat retinal ganglion cells during prenatal life. *Proceedings of the National Academy of Sciences of the United States of America*, *87*(7), 2861–2864. https://doi.org/10.1073/pnas.87.7.2861

McLaughlin, T., Torborg, C. L., Feller, M. B., & O'Leary, D. D. M. (2003). Retinotopic map refinement requires spontaneous retinal waves during a brief critical period of development. *Neuron*, *40*(6), 1147–1160. https://doi.org/10.1016/S0896-6273(03)00790-6

McNeill, D. S., Sheely, C. J., Ecker, J. L., Badea, T. C., Morhardt, D., Guido, W., & Hattar, S. (2011). Development of melanopsin-based irradiance detecting circuitry. *Neural Development*, *6*(1), 2–11. https://doi.org/10.1186/1749-8104-6-8

Meister, M., Wong, R. L., Baylor, D. a, & Shatz, C. J. (1991). *Action the*. *May*.

Rao, S., Chun, C., Fan, J., Kofron, J. M., Yang, M. B., Hegde, R. S., Ferrara, N., Copenhagen, D. R., & Lang, R. A. (2013). A direct and melanopsin-dependent fetal light response regulates mouse eye development. *Nature*, *494*(7436), 243–246. https://doi.org/10.1038/nature11823

Ray, T. A., Roy, S., Kozlowski, C., Wang, J., Cafaro, J., Hulbert, S. W., Wright, C. V, Field, G. D., & Kay, J. N. (2018). Formation of retinal direction-selective circuitry initiated by starburst amacrine cell homotypic contact. *ELife*, 1–44. doi: https://doi.org/10.7554/eLife.34241

Rosa, J. M., Bos, R., Sack, G. S., Fortuny, C., Agarwal, A., Bergles, D. E., Flannery, J. G., &

Feller, M. B. (2015). Neuron-glia signaling in developing retina mediated by neurotransmitter spillover. *ELife*, *4*(AUGUST2015), 1–20. https://doi.org/10.7554/eLife.09590

Shekhar, K., Whitney, I. E., Butrus, S., Peng, Y.-R., & Sanes, J. R. (2022). Diversification of multipotential postmitotic mouse retinal ganglion cell precursors into discrete types. *ELife*, *11*. https://doi.org/10.7554/eLife.73809

Summers, M., El Quessney, M., & Feller, M. (2021). Retinal Mechanisms for Motion Detection. *Oxford Research Encyclopedia of Neuroscience*. https://doi.org/10.1093/acrefore/9780190264086.013.356

Syed, M. M., Lee, S., Zheng, J., & Zhou, Z. J. (2004). Stage-dependent dynamics and modulation of spontaneous waves in the developing rabbit retina. *Journal of Physiology*, *560*(2), 533–549. https://doi.org/10.1113/jphysiol.2004.066597

Tian, N., & Copenhagen, D. R. (2003). Visual stimulation is required for refinement on ON and OFF pathways in postnatal retina. *Neuron*, *39*(1), 85–96. https://doi.org/10.1016/S0896-6273(03)00389-1

Tiriac, A., Smith, B. E., & Feller, M. B. (2018). Light Prior to Eye Opening Promotes Retinal Waves and Eye-Specific Segregation. *Neuron*, *100*(5), 1059-1065.e4. https://doi.org/10.1016/j.neuron.2018.10.011

Whitney, I. E., Butrus, S., Dyer, M. A., Rieke, F., Sanes, J. R., & Shekhar, K. (2022). Vision-Dependent and -Independent Molecular Maturation of Mouse Retinal Ganglion Cells. *Neuroscience*. https://doi.org/10.1016/j.neuroscience.2022.07.013

Wong, R. O. (1999). Retinal waves: stirring up a storm. *Neuron*, *24*(3), 493–495.

Yan, W., Laboulaye, M. A., Tran, N. M., Whitney, I. E., Benhar, I., & Sanes, J. R. (2020). Mouse Retinal Cell Atlas: Molecular Identification of over Sixty Amacrine Cell Types. *Journal of Neuroscience*, *40*(27), 5177–5195. https://doi.org/10.1523/JNEUROSCI.0471-20.2020

Chapter 2

Circuit Mechanisms Underlying Embryonic Retinal Waves

Publication related to this work:
This chapter is a full reprint of Voufo, Chen, Smith, Yan, Feller, Tiriac, under revision at *Elife* (2022), of which I was the primary author. This work is included with permission from all authors.

Voufo, C., Chen, A.Q., Smith, B.E., Yan, R.S., Feller, M.B., Tiriac, A., (2022). Circuit Mechanisms Underlying Embryonic Retinal Waves**.** *BioRxiv*. 2022.0814.503889. https://doi.org/10.1101/2022.08.14.503889

SUMMARY

Spontaneous activity is a hallmark of developing neural systems. In the retina, spontaneous activity comes in the form of retinal waves, comprised of three stages persisting from embryonic day 16 (E16) to eye opening at postnatal day 14 (P14). Though postnatal retinal waves have been well characterized, little is known about the spatiotemporal properties or the mechanisms mediating embryonic retinal waves, designated Stage 1 waves. Using a custom-built macroscope to record spontaneous calcium transients from whole embryonic retinas, we show that Stage 1 waves are initiated at several locations across the retina and have a broad distribution of propagation areas. A gap junction antagonist, meclofenamic acid, reduced the frequency and size of Stage 1 waves, nearly abolishing them. The general nAChR antagonist, hexamethonium similarly nearly abolished Stage 1 waves. Application of the α4β2 nAChR antagonist dihydro-ß-erythroidine only slightly reduced the frequency of waves but significantly reduced the number of cells that participated in waves. Thus, Stage 1 waves are mediated by a complex circuitry involving subtypes of nAChRs and gap junctions. Stage 1 waves in mice lacking the β2 subunit of the nAChRs (β2-nAChR-KO) were reduced, but in contrast to WT mice, they persisted in hexamethonium and were completely blocked by meclofenamic acid. To assay the impact of Stage 1 waves on retinal development, we compared the spatial distribution of a subtype of retinal ganglion cells, intrinsically photosensitive retinal ganglion cells (ipRGCs), which undergo a significant amount of cell death, in WT and β2-nAChR-KO mice. We found that the developmental decrease of ipRGC density is preserved between WT and β2-nAChR-KO mice, indicating that processes regulating ipRGC distribution are not influenced by spontaneous activity.

INTRODUCTION

Throughout the developing nervous system, spontaneous activity is observed before neural circuits are fully formed and sensory transduction begins (Akin & Zipursky, 2020; Blankenship & Feller, 2010; Luhmann & Khazipov, 2018; Spontaneous Activity in Developing Thalamic and Cortical Sensory Networks, 2021). This activity is implicated in several development events, including cell death, maturation of functional circuits, and refinement of projection neurons in their targets in the brain (Blanquie, Kilb, et al., 2017; Fujimoto et al., 2019; Kirkby et al., 2013). This is well studied in the developing visual system, where prior to the maturation of vision, laterally propagating spontaneous depolarizations sweep across retinal ganglion cells (RGCs), a pattern referred to as retinal waves (Wong, 1999). Retinal waves drive eye specific segregation and retinotopic refinement of retinal projections to the dorsal lateral geniculate nucleus of the thalamus and superior colliculus (Ackman & Crair, 2014; Arroyo & Feller, 2016). Retinal waves also play a role in the maturation of direction selective circuits within the retina itself (Tiriac et al., 2022) as well as the development of retinal vasculature (Biswas et al., 2020; Weiner et al., 2019).

Retinal waves are present throughout mouse retinal development, starting as early as embryonic day 16 and persisting until postnatal day 14, which is around the time of eye opening (Blankenship & Feller, 2010; Choi et al., 2021; Feller & Kerschensteiner, 2013). As the retina develops, the circuits that mediate waves change. Stage 2 retinal waves, observed between postnatal day 1 and 10 (P1-10), are mediated via activation of nicotinic acetylcholine receptors (nAChRs) by acetylcholine (ACh) released from starburst amacrine cells (SACs). Stage 3 retinal waves, observed between P10-14, are mediated via activation of ionotropic glutamate receptors by glutamate released from bipolar cells.

Stage 1 waves are observed between embryonic day 16 and 18 (E16-18) (Bansal et al., 2000) while in rabbit they are present at E22 (Syed et al., 2004) are perhaps the least well understood yet they are concurrent with many important events in retinal development as well as retinal projections to the brain (Spontaneous Activity in Developing Thalamic and Cortical Sensory Networks, 2021). In rabbit, Stage 1 waves persist in the presence of pharmacological antagonists of fast neurotransmitters and are blocked by gap junction antagonists (Syed et al., 2004). In mice, Stage 1 waves consist of large propagating waves and small non-propagating transients (Bansal et al., 2000). The application of nAChR antagonist inhibits larger propagating waves (Bansal et al., 2000). Though there is no anatomical evidence of synapses as early as E16-18, recent work has shown that SACs are present embryonically, begin to migrate to the inner nuclear layer (INL), and send projections to the inner plexiform layer (IPL) guided by homotypic contacts (Ray et al., 2018). Hence cholinergic signaling is likely occurring via the volumetric release of ACh. Exactly how gap junctions and cholinergic signaling set the spatiotemporal properties of Stage 1 waves remains to be understood.

Here we describe the spatiotemporal properties of Stage 1 waves across the whole retina using a novel macroscope. We then identify the role of gap junction and cholinergic circuits on the generation and propagation of Stage 1 waves. Next, we explore Stage 1 waves in the β2-nAChR-KO mouse, which is the canonical mouse model for the studying the role of Stage 2 waves in developmental processes, and report that this mouse also exhibits altered Stage 1 activity. Finally, we use β2-nAChR-KO mice to demonstrate that the regulation of ipRGC number is a wave-independent process.

RESULTS

Macroscope imaging reveals the spatiotemporal properties of Stage 1 retinal waves

The mouse retina at E16-18 exhibits spontaneous correlated activity (Bansal et al., 2000; Syed et al., 2004), termed Stage 1 retinal waves, despite the immature state of retinal circuits. At E16-18, several postmitotic cell types are present in the retina, including broad classes of retinal ganglion cells (RGCs) and amacrine cells (ACs), as well as proliferating progenitors which will go on to produce cells such as rods, bipolar cells, and Muller glia postnatally (Fig 1A)(Cepko, 2014). By E17, there are no chemical synaptic structures (Hoon et al., 2014), though migrating SACs release ACh (Wong, 1995) and they, along with RGCs, express nicotinic acetylcholine receptors. One potential mode of cell-cell communication is via gap junction coupling between RGCs as well as between progenitor cells (Cook & Becker, 2009), which have been proposed to be the primary substrate mediating Stage 1 waves (Catsicas et al., 1998; Syed et al., 2004; Wong et al., 1998).

To understand how cholinergic signaling and gap junction coupling govern Stage 1 waves, we first imaged large quantities of Stage 1 waves to better understand their spatiotemporal properties. Retinas were isolated from E16-18 mice that were either bath loaded with the organic calcium dye Cal 520, or from mice expressing the genetically encoded calcium indicator GCaMP6s under the *Vglut2* promoter (Vglut2::GCaMP6s). The earliest age at which we could detect reliable waves was E16 (Supp Movie 1). Stage 1 retinal waves were recorded on retinal whole-mounts, using a custom built epifluorescent macroscope.

To assess the spatiotemporal properties of Stage 1 waves, we divided the retinal surface into small square ROIs (roughly 10 µm x10 µm), about 7 µm apart. $\Delta F/F$ traces for each ROI were rasterized based on a detection algorithm which identified the timing of peak changes in fluorescence, which we call transients (Figure 1B). These rasterized transients were used for subsequent analysis. We first computed the time between spontaneous transients by measuring the inter-transient interval (ITI) for each ROI and found that the distribution peaked at around 80 seconds (Figure 1C). We also described the size of individual waves by computing the sum of transients that occurred simultaneously (i.e., percent of ROIs that participated in each wave). The distribution of wave sizes was broad, ranging from 6% to 90% of the retina, with a mean and standard deviation of 46 ± 21% (Figure 1D).

In addition to propagating waves, we also observed small non-propagating calcium events (defined by transients present in a few neighboring ROIs that never propagated beyond 160x160 μm^2) (Supp Movie 2 Figure 1-supplement 1). These events were like those described previously

in (Bansal et al., 2000). Note, these small non-propagating transients were included in the ITI but not in the analysis of propagating wave sizes.

Finally, we calculated the average propagation speed of Stage 1 waves to range from 136 μm/s to 302 μm/s (Average ± SD: 181 ± 24 μm/s) (Figure 1E, Figure1-Supplement 2), with an average speed of 190 μm/s ± 38 μm/s (see Table 1 for wave speed summary data). We also measured the distribution of Stage 1 wave initiation sites in WT retinas and saw no evidence of an initiation site bias (Figure 1-supplement 3).

nAChRs and gap junctions are important for setting the frequency and area of Stage 1 waves

Previous work based on epifluorescent calcium imaging experiments performed in embryonic mice has shown that retinal waves, as defined by correlated changes in fluorescence, are reduced in frequency and size by curare, a competitive antagonist for nAChRs (Bansal et al., 2000). However, in roughly the equivalent developmental period in rabbit, blockade of all fast neurotransmitter receptor, including nAChRs, had no impact on wave frequency (Syed et al, 2004). Rather, waves in rabbit are blocked after the application of 18β-glycyrrhetinic acid, a gap junction antagonist (Syed et al., 2004).

To determine the relative role of gap junctions and nAChRs on the frequency and area of Stage 1 waves in mice, we used two-photon calcium imaging and pharmacology in retinas isolated from E16-18 mice bath loaded with Cal 520. To block gap junctions, we bath applied the gap junction antagonist meclofenamic acid (MFA, 50μM), which reversibly blocks electrical coupling between retinal interneurons (Veruki & Hartveit, 2009) and developing ipRGCs (Caval-Holme & Feller, 2019). Application of the gap junction blocker meclofenamic acid (MFA, 50μM) nearly abolished Stage 1 waves, causing a significant reduction in frequency of waves and cell participation during waves (Figure 2A-C). We also found a small but significant reduction in wave amplitude, quantified as the average maximum response amplitude of all cells participating in individual waves (Figure 2D).

MFA has notable off-target effects including overall cell health after long exposures (Kuo et al., 2016). Previous studies from our lab show that at P6, MFA does not reduce light-induced calcium transients in M1-iRGCs, the ability of M4-ipRGCs to fire action potentials nor the amplitude of depolarization -induced calcium transients. Note this is in contrast to another gap junction antagonist, carbenoxolone, which inhibits light responses in cultured ipRGCs (Bramley et al., 2011). Here, we have assayed the impact of MFA on voltage-gated ion channels on RGCs in E16-E18 retina but found inconsistent results (Figure 2, Supplement 1). We associate this high variance with a rapid changing complements of ion channels during development and the quick

washout of these conductances during whole cell recordings. Hence, we conclude that MFA's block on retinal waves is via their impact on gap junctions.

We next assayed the impact on nAChR-antagonists on Stage 1 waves. For Stage 2 waves, both spontaneous calcium transients and compound excitatory synaptic events are completely blocked by bath application of dihydro-ß-erythroidine hydrobromide (DHβE, 8μM) (Ford et al., 2012), which preferentially targets nAChRs containing α4 and β2-subunits (Harvey et al., 1996; Harvey & Luetje, 1996). We found that DHβE also dramatically reduced activity associated with Stage 1 retinal waves (Figure 2E). However, in contrast to Stage 2 wave, some waves persisted in the presence of DhβE (Figure 2F), but they recruited fewer neurons and therefore had smaller areas (Figure 2G). DhβE did not significantly reduce the activity of the neurons that participated in the remaining waves (Figure 2H). Stage 1 waves were blocked by general nAChR antagonists: both hexamethonium (Figure 2I-J; Hex, 100μM), a non-selective nAChR antagonist, as well as in epibatidine (Figure 2K-L; EPB, 10 nM), a nAChR agonist that potently desensitizes all nAChRs (Corrie et al., 2020; Spang et al., 2000) blocked Stage 1 waves. Hence, Stage 1 waves are mediated in initiation and propagation of Stage 1 waves both gap junctions and multiple subunit combinations of nAChRs.

β2-nAChR knock-out mice exhibit perturbed Stage 1 waves

Our results thus far indicate that both the frequency and area of Stage 1 retinal waves are modulated by the activation of different subtypes of nAChRs as well as gap junction coupling. To further differentiate the role of different nAChRs, we characterized mice where the β2 subunit of the nicotinic acetylcholine receptor is genetically ablated (β2-nAChR-KO). β2-nAChR-KO mice have severely disrupted Stage 2 retinal waves (Bansal et al., 2000; Rossi et al., 2001) and have served as a model system for assessing the role of Stage 2 waves in driving different developmental events (Ackman et al., 2012; Burbridge et al., 2014).

We observed that β2-nAChR-KO retinas exhibited Stage 1 waves with different spatiotemporal properties than WT retinas (Figure 3A&B, see also Supp Movie 3). Specifically, β2-nAChR-KO retinas exhibited longer ITIs (Figure 3C-D), and individual waves propagated over smaller areas β2-nAChR-KO (Figure 3E and Figure 1-Supplement 1). In sharp contrast to WT retina, waves in the β2-nAChR-KO retina were unaffected by the addition of Hex but showed a significant reduction in both area and frequency with the application of MFA. These results suggest that in the absence of β2-nAChRs, gap junctions become a major component of the Stage 1 wave generation mechanism. Furthermore, we found that Stage 1 waves in the β2-nAChR-KO propagated at a significantly slower speed than those observed in WT mice, (Average ± SD: 99 ± 15 μm/sec compared to 181 ± 24 μm/sec for WT, n= 10 waves per condition, $p = 3.9073e^{-8}$) (Figure 3F), consistent with a distinct mechanism of propagation.

Finally, we wanted to test whether the properties of Stage 1 waves in WT or β2-nAChR-KO were influenced by light activation of ipRGCs via the 474 nm imaging light used to excite the calcium dye on the macroscope. ipRGCs have been shown to be responsive to 476 nm light during both embryonic and postnatal development (Emanuel & Do, 2015; Verweij et al., 2019). Previous studies have shown a light dependent increase in the wave frequency of Stage 2 waves in the β2-nAChR-KO during the first postnatal week (Kirkby & Feller, 2013). This light modulation of the spatiotemporal properties of β2-nAChR-KO during the first postnatal week depends on ipRGC melanopsin expression, as well as an increase in gap junction conductance between ipRGCs and other RGCs (Arroyo et al., 2016; Kirkby & Feller, 2013). However, we found no difference in the frequency of waves recorded using a two-photon microscope (based on 920 nm illumination) to those recorded on the macroscope and in either the WT or β2 nAChR-KO embryonic retinas (Figure 3 Supplement 1). Hence, we conclude that light activation of ipRGCs does not significantly influence the spatiotemporal properties of Stage 1 retinal waves in either WT or the β2 nAChR-KO retinas. These results are consistent with the fact that light stimulation of the retina does not modulate the frequency of Stage 2 waves and only begins to do so when conventional photoreceptors come online during Stage 3 waves (Tiriac et al., 2018).

ipRGCs participate in Stage 1 waves but their number and distribution are not altered in the β2-nAChRs-KO

RGCs undergo a period of dramatic cell death during the first two postnatal weeks of development, the majority occurring during the first postnatal week (Abed et al., 2022; Braunger et al., 2014). Whether this cell death process is regulated by retinal waves is unknown. We looked specifically at intrinsically photosensitive ganglion cells (ipRGCs) for several reasons. First, ipRGCs have completed proliferation (Lucas & Schmidt, 2019; McNeill et al., 2011) and appear to be fully differentiated by E16 (Shekhar et al., 2022; Whitney et al., 2022), the onset of Stage 1 waves. ipRGCs undergo a period of dramatic cell death during the first two postnatal weeks of development, the majority occurring during the first postnatal week, prevention of which profoundly disrupts several important developmental processes in the retina – including spacing of ipRGC somas as well as rod and cone mediated circadian entrainment through the activation of ipRGCs (Chen et al., 2013). However, the exact mechanism regulating ipRGC cell death is unknown. Here we assessed the impact of disrupting Stage 1 and Stage 2 waves on the number and distribution of ipRGCs.

We first set out to determine whether ipRGCs participate in Stage 1 waves. To do this, we conducted two-photon calcium imaging of RGCs in the ganglion cell layer (GCL) of retinas isolated from $Opn4^{Cre/+}$; $tdTomato^{fl/fl}$ E16-18 mice (Ecker et al., 2010), which express tdTomato in ipRGCs (Figure 4A) enabling us to assess the differential participation of RGCs and ipRGCs during Stage 1 waves (Figure 4B). On average, both RGCs and ipRGCs participated in most waves with no significant differences between the two groups (Figure 4C; Average ±SD: RGCs

78.78±21.48%; ipRGCs 84.64±16.86%). We also found no significant differences in the amplitude of the calcium response that RGCs and ipRGCs exhibit in response to Stage 1 waves (Figure 4D). Hence, ipRGCs are depolarized by Stage 1 waves similarly to Stage 2 waves (Caval-Holme & Feller, 2019; Caval-Holme et al., 2022; Chew et al., 2017).

Since β2-nAChR-KO retinas exhibited reduced retinal activity during both embryonic and early postnatal development, we used this mouse as a model to determine whether normal Stage 1 and Stage 2 wave activity is important for regulating the number and distribution of ipRGCs. To this end, we isolated retinas from $Opn4^{Cre/+}$;$tdTomato^{fl/fl}$ and $Opn4^{Cre/+}$;$tdTomato^{fl/fl}$;($\beta2\text{-nAChR}^{-/-}$) at P1 and P7. These retinas express tdTomato in all melanopsin-expressing cells regardless of subtype. Retinas were imaged using wide-field epifluorescence microscopy (Figures 5A and B).

We observed a dramatic decrease in the density of ipRGCs in WT retinas from P1 to P7 (Figures 5B, C; $p = 1.17x10^{-7}$), consistent with previous studies of ipRGCs (Chen et al., 2013) and which coincides with peak levels of RGC apoptosis, the primary cause of RGC death during development (Braunger et al., 2014; Young, 1984). We found that β2-nAChR-KO retinas exhibited the same density of ipRGCs at P1 as WT retinas, suggesting that the decrease in activity in Stage 1 waves does not regulate ipRGC cell density. Like WTs, β2-nAChR-KO retinas also exhibited a decrease in the density of ipRGCs from P1 to P7 ($p = 4.99x10^{-11}$). At P7, we observed a small but significant increase in ipRGC densities at P7 in β2-nAChR-KO mice than in WT mice (568± 33 ipRGCs/μm^2 in WT vs 654 ± 78 ipRGCs/μm^2 in β2-nAChR-KO, n= 8 retinas in each genotype; $p = 0.012$). We cannot determine whether this small difference is due to the smaller size of retinas in β2-nAChR-KO retinas (Xu et al., 1999) or reflects a true increase in cell number. Overall, these data indicate that the cell death processes that regulate ipRGC number during the first postnatal week are not strongly dependent on retinal waves.

To determine the impact of this developmental decrease in cell density on the mosaic organization of ipRGCs, we computed the regularity index, which is equal to the average nearest neighbor distance divided by the standard deviation. A high regularity index is associated with a non-random distribution of somas. Despite the expected increase in nearest neighbor distance in WT and β2-nAChR-KOs retina between P1 and P7 (Figure 5D, see Table 2), there was only a small decrease in the regularity index. Interestingly, the measured mean regularity indices of 2.8 ± 0.12 (WT P1), 2.9 ± 0.16 (β2-nAChR-KO P1), 2.3 ± 0.13 (WT P7), and 2.6 ± 0.2 (β2-nAChR-KO P1) are random, as they fall within the range of what would be predicted by a random distribution of cells with soma diameters between 7-10 μm (Keeley et al., 2020). Hence the decrease in cell density does not appear to make the soma organization more ordered. This might be expected, since our analysis does not differentiate between ipRGC subtypes, each of which likely forms an independent retinal mosaic. Together these data indicate that although retinal waves provide a robust source of depolarization for embryonic and early postnatal ipRGCs, reducing wave activity does not significantly influence the cell death process.

DISCUSSION

We show that Stage 1 retinal waves are a robust source of spontaneous activity in the embryonic retina. Stage 1 waves initiate throughout the retina, propagate over finite regions of varying size and drive periodic depolarizations of neurons in the immature retinal ganglion cell layer. In WT embryonic mice, the frequency of Stage 1 wave is abolished in the presence of general nAChR antagonists but persists, albeit with greatly reduced cell participation, in a nAChR antagonist that targets α4β2 containing nAChRs. In the presence of gap junction antagonists, the frequency and participation of cells within waves is greatly diminished, though some waves still occur. We found that the β2-nAChR-KO mouse, which exhibits strongly reduced Stage 2 wave frequency, does not exhibit the same dramatic reduction in frequency embryonically in control conditions and in the presence of a general nAChR antagonist, though the area of waves are greatly diminished. However, similar to what we observed in WT mice, the frequency of Stage 1 waves in β2-nAChR-KO mice were greatly reduced in the presence of a gap junction antagonist. This more striking effect of the gap junction antagonist compared to the general nAChR antagonist, indicates that the electrical synapses may compensate for a lack of at least some nAChRs in β2-nAChR-KO mice. Finally, we showed that ipRGCs are depolarized by Stage 1 waves, but that decreasing number of ipRGCs across early postnatal development was unaffected in the β2-nAChR-KO mouse, indicating that the proliferation and cell death processes that influence ipRGC number are not dependent on wave activity.

Distinctions and similarities between Stage 1 and Stage 2 waves

Our findings support a model in which there are both key differences and some similarities between Stage 1 and 2 waves. The distribution of ITI is peaked at roughly 80 seconds for Stage 1 waves which is a slightly longer interval than the peak interval reported for Stage 2 (compare Figure 1C here to Figure 7D in Ford et al, 2012). Stage 1 and 2 waves also propagate at similar speeds. Key differences are that spontaneous activity between E16 and E18 included small non-propagating transients and propagating waves of a broad range of sizes. In contrast, after P1, there are no small non-propagating transients, and Stage 2 waves mostly propagate over large areas of the retina, as observed both *in vitro* (Feller et al., 1997; Hilgen et al., 2017) and *in vivo* (Ackman et al., 2012). Note the spatiotemporal properties of Stage 2 waves also vary dramatically across the developmental period spanning P1-P10 (Ge et al., 2021; Hilgen et al., 2017) and therefore we are making these comparisons to the earlier Stage 2 waves.

The similarity in frequency of waves and propagation speed indicate that the mechanisms responsible for initiating and propagating large waves are similar for Stage 1 and 2 waves. Indeed, Stage 1 and 2 waves share a dependence on nAChR signaling. Starburst amacrine cells (SACs) are the sole source of ACh in the retina. During the period of development concurrent with Stage 1 waves, SACs begin to migrate toward the INL and send projections to the IPL via

homotypic contacts (Ray et al., 2018). Also during this period, SACs start to express choline acetyltransferase at E17 in the rat retina (Kim et al., 2000), equivalent to E15.5 in mice (Schneider & Norton, 1979), and show a response to nicotine in the fetal rabbit retina between E20-27 (Wong, 1995), corresponding to Stage 1 and 2 waves in rabbit (Syed et al., 2004). Together these studies support the idea that during embryonic development, SACs are not only releasing ACh but also forming a cholinergic network, similar to that of Stage 2 wave propagation (Ford & Feller, 2012). Here, we have shown that Stage 1 waves fail to initiate in the presence of the general nAChR antagonists, hexamethonium (Hex) and epibatidine (EPB). This suggests that spontaneous depolarization of SACs is important for wave initiation and that the cholinergic circuits that mediates waves start earlier than expected.

One key difference in ACh signaling between Stage 1 and 2 waves is their sensitivity to the specific nAChR antagonist, DhβE Though DHβE reduced the number of Stage 1 waves, many smaller calcium transients persisted. In contrast, DHβE is a potent blocker of all activity during Stage 2 waves (Ford et al., 2012). DHβE is an nAChR antagonist with a greater affinity for nAChRs containing α4 and β2 subunits in heterologous systems (Ho et al., 2020; Papke et al., 2010). The fact that all Stage 1 wave activity is blocked by Hex and EPB suggests that different subunit combinations of nAChRs, on both SACs and RGCs, are independently contributing to either the initiation or propagation of Stage 1 waves.

The different sensitivity to nAChR antagonists between Stage 1 and 2 waves is highlighted in the patterns of retinal waves in β2-nAChR-KO mice. β2-nAChR-KO mice have significantly reduced Stage 2 cholinergic waves (Bansal et al., 2000; Burbridge et al., 2014; Xu et al., 2015, 2016) and as such have served as the canonical model for studying the role of Stage 2 cholinergic waves in eye-specific segregation, retinotopic maps, retinal and collicular direction selectivity, and in the optokinetic reflex (Arroyo & Feller, 2016; Grubb et al., 2003; Thompson et al., 2017; Tiriac et al., 2022; Wang et al., 2009). In contrast, Stage 1 waves in the β2-nAChR-KO mice persist, albeit they propagate with slower speed and cover smaller areas of the retina (Figure 3). Despite this difference in spatiotemporal properties, both Stage 1 and Stage 2 waves that persist in the β2-nAChR-KO mice are blocked by gap junction receptor antagonist rather than blockers of fast neurotransmitter receptors (Kirkby & Feller, 2013). Recent evidence suggests that embryonic activity throughout developing sensory system may influence many aspects of visual systems development (Spontaneous Activity in Developing Thalamic and Cortical Sensory Networks, 2021; Moreno-Juan et al., 2022). Whether the various visual system phenotypes observed in β2-nAChR-KO mice can be attributed in part to reduced Stage 1waves remains to be determined.

In our hands, global blockade or desensitization of nAChRs completely abolished Stage I waves. This result appears to conflict with previous studies in mice showing that application of curare, a competitive antagonist for nAChRs, preserves small non-propagating transients (Bansal et al., 2000). One possibility is that in contrast to hexamethonium, curare has mixed affinity for

neuronal nAChRs. A second is that curare was acting via other neurotransmitter receptors where it has some cross-reactivity not shared by the receptor antagonists that we used (Spirova et al., 2019; Wotring & Yoon, 1995).

In addition to the ACh signaling, gap junctions also play a role in mediating Stage 1 retinal waves. Here we use the gap junction antagonist meclofenamic acid (MFA), which was previously shown to reversibly block junctional conductance (Veruki & Hartveit, 2009), dye coupling (Pan et al., 2007) and spikelets between developing RGCs (Caval-Holme & Feller, 2019). Application of MFA led to a significant reduction in both the frequency and size of Stage 1 waves. The results we observed in MFA are consistent with the pharmacological studies of Stage 1 waves in other species: Stage 1 waves in rabbit are insensitive to nAChR antagonists (Syed et al., 2004), as are early waves in developing chick retina (Catsicas et al., 1998). Note that waves in these species were also sensitive to antagonists of various metabotropic receptors, indicating that neurotransmitters are still important for propagating waves in these systems. However, there is the important caveat that MFA can also have some off-target effects that might impact wave propagation (Kuo et al., 2016). Previously we should that in P6-7 retina, MFA did not alter depolarization induced calcium transients and did not reduced the excitability of RGCs. Here we show that short applications(10 minutes) of MFA increased input resistance of RGCs and did not appear to block compound EPSCs associated with waves or voltage-gated sodium and potassium channels. Future experiments independent measures of gap junction coupling – such as tracer coupling and potentially knockout of connexin proteins are necessary to have a more complete understanding of how electrical synapses contribute to wave propagation properties.

We also observed a difference between Stage 1 and 2 waves in β2-nAChR-KO retinas. Embryonic β2-nAChR-KO retinas still exhibited Stage 1 waves but at reduced frequency and size when compared to WT retinas. Though the spatiotemporal properties of Stage 2 waves recorded *in vitro* for P1-P8 β2-nAChR-KO retinas is highly dependent on recording conditions with results ranging from sparse activity to high frequency (Bansal et al., 2000; Stafford et al., 2009; Xu et al., 2016), *in vivo* waves in β2-nAChR-KO are infrequent and weakly depolarizing (Burbridge et al., 2014). The activity that persists in β2-nAChR-KO retinas both embryonically and postnatally is resistant to nAChR antagonists, as was observed previously (Bansal et al., 2000). Rather the remaining activity in β2-nAChR-KO retinas is completely blocked by MFA, therefore suggesting that stage 1 and 2 waves in β2-nAChR-KO retinas rely solely on gap junctions (Kirkby & Feller, 2013).

We propose a model for Stage 1 waves consistent with these observations (Figure 6). Stage 1 wave initiation is dependent on the spontaneous depolarization of SACs, but wave propagation is dependent on both gap junction coupling and nAChR activation. Hence Stage 1 wave initiation is similar to Stage 2 waves where the spontaneous depolarization of a SAC activates neighboring SACs, leading to the volumetric release of ACh responsible for wave propagation both in the

INL and GCL (Ford et al., 2012). The model for Stage 1 wave propagation is similar to Stage 2 wave propagation, though a complete description of how gap junction coupling is mediating Stage 2 wave propagation is needed. The pharmacological and genetic block/ablation of gap junctions have yet to reveal a phenotype (Blankenship et al., 2011; Caval-Holme & Feller, 2019; Kirkby & Feller, 2013; Singer et al., 2001; Torborg et al., 2005). Interestingly, pure gap junction mediated waves, such as those we observed in the β2-nAChR KO mouse, are considerably slower than waves in WT retina. A recent computational model of gap junction mediated Stage 1 waves, where waves are initiated by RGCs undergoing rare and random depolarizations that propagate entirely via electrical synapses, argues that the speed of propagation is limited by the slow rate at which the junctional currents charge up the membrane capacitance of neighboring RGCs (Kähne et al., 2019). Hence the faster speed of waves mediated by a combination of nAChRs and gap junctions indicates that diffuse release of ACh leads to faster propagation than electrical synapses alone.

Interactions between Stage 1 waves and ipRGCs

Early intrinsic light responses of ipRGCs have been implicated in several developmental events (Aranda & Schmidt, 2021), including retinal vascularization (Rao et al., 2013), maturation of circadian circuits (McNeill et al., 2011) and the maturation of the lens to prevent myopia (Chakraborty et al., 2022). Here we report that ipRGCs are robustly activated by Stage 1 waves, similar to our observations that ipRGCs participate in Stage 2 waves (Arroyo et al., 2016; Caval-Holme et al., 2022; Kirkby & Feller, 2013). Thus, it is possible that depolarization via Stage 1 waves may contribute to some of these ipRGC-dependent developmental processes.

To begin to explore to role of Stage 1 and 2 waves in ipRGC development, we monitored the impact of chronically altered waves on the distribution and number of ipRGCs across the retina. Notably, ipRGCs undergo extensive apoptotic cell death, with the peak of apoptosis occurring between P2-P4 (Chen et al., 2013). Prevention of apoptosis during this developmental period doubles the number of ipRGCs and dramatically increases the clumping of M1-ipRGC somas. In some systems, correlated network activity has been implicated in cell proliferation and cell death. For example, retinal wave activity promotes neurite outgrowth and potentially survival among RGCs (Goldberg et al., 2002). Additionally, in the developing primary somatosensory and motor cortices, higher levels of spontaneous electrical activity were shown to have a neuroprotective effect (Blanquie, Yang, et al., 2017). However, here we show in the β2-nAChR-KO mouse, which has significantly diminished Stage 1 and 2 retinal waves, the normal developmental loss of ipRGCs between P1 and P7 is maintained. Thus, Stage 1 and 2 retinal waves are not required for ipRGC apoptosis; however, it is possible that the residual wave activity in β2-nAChR-KO is sufficient to activate pro-survival pathways. A deeper understanding of how spontaneous activity modulates RGC survival pathways (e.g. (Ahmed et al., 2022) is warranted.

REFERENCES

Abed, S., Reilly, A., Arnold, S. J., & Feldheim, D. A. (2022). Adult Expression of Tbr2 Is Required for the Maintenance but Not Survival of Intrinsically Photosensitive Retinal Ganglion Cells. *Frontiers in Cellular Neuroscience*, *16*, 101. https://doi.org/10.3389/fncel.2022.826590

Ackman, J. B., Burbridge, T. J., & Crair, M. C. (2012). Retinal waves coordinate patterned activity throughout the developing visual system. *Nature*, *490*(7419), 219–225. https://doi.org/10.1038/nature11529

Ackman, J. B., & Crair, M. C. (2014). Role of emergent neural activity in visual map development. *Current Opinion in Neurobiology*, *24*, 166–175. https://doi.org/10.1016/j.conb.2013.11.011

Ahmed, M., Kojima, Y., & Masai, I. (2022). Strip1 regulates retinal ganglion cell survival by suppressing Jun-mediated apoptosis to promote retinal neural circuit formation. *ELife*, *11*. https://doi.org/10.7554/eLife.74650

Akin, O., & Zipursky, S. L. (2020). Activity regulates brain development in the fly. In *Current Opinion in Genetics and Development* (Vol. 65, pp. 8–13). Elsevier Ltd. https://doi.org/10.1016/j.gde.2020.04.005

Aranda, M. L., & Schmidt, T. M. (2021). Diversity of intrinsically photosensitive retinal ganglion cells: circuits and functions. *Cellular and Molecular Life Sciences*, *78*(3), 889–907. https://doi.org/10.1007/s00018-020-03641-5

Arroyo, D. A., & Feller, M. B. (2016). Spatiotemporal features of retinal waves instruct the wiring of the visual circuitry. *Frontiers in Neural Circuits*, *10*(JUL2016), 54. https://doi.org/10.3389/fncir.2016.00054

Arroyo, D. A., Kirkby, L. A., & Feller, M. B. (2016). Retinal waves modulate an intraretinal circuit of intrinsically photosensitive retinal ganglion cells. *Journal of Neuroscience*, *36*(26), 6892–6905. https://doi.org/10.1523/JNEUROSCI.0572-16.2016

Bansal, A., Singer, J. H., Hwang, B. J., Xu, W., Beaudet, A., & Feller, M. B. (2000). Mice Lacking Specific Nicotinic Acetylcholine Receptor Subunits Exhibit Dramatically Altered Spontaneous Activity Patterns and Reveal a Limited Role for Retinal Waves in Forming ON and OFF Circuits in the Inner Retina. *Journal of Neuroscience*, *20*(20), 7672–7681. https://www.jneurosci.org/content/20/20/7672.long

Biswas, S., Cottarelli, A., & Agalliu, D. (2020). Neuronal and glial regulation of CNS angiogenesis and barriergenesis. In *Development (Cambridge)* (Vol. 147, Issue 9). Company of Biologists Ltd. https://doi.org/10.1242/dev.182279

Blankenship, A.G., Hamby, A. M., Firl, A., Vyas, S., Maxeiner, S., Willecke, K., & Feller, M. B.

(2011). The role of neuronal connexins 36 and 45 in shaping spontaneous firing patterns in the developing retina. *Journal of Neuroscience*, *31*(27). https://doi.org/10.1523/JNEUROSCI.5640-10.2011

Blankenship, Aaron G., & Feller, M. B. (2010). Mechanisms underlying spontaneous patterned activity in developing neural circuits. *Nature Reviews Neuroscience*, *11*(1), 18–29. https://doi.org/10.1038/nrn2759

Blanquie, O., Kilb, W., Sinning, A., & Luhmann, H. J. (2017). Homeostatic interplay between electrical activity and neuronal apoptosis in the developing neocortex. In *Neuroscience* (Vol. 358, pp. 190–200). Elsevier Ltd. https://doi.org/10.1016/j.neuroscience.2017.06.030

Blanquie, O., Yang, J.-W. W., Kilb, W., Sharopov, S., Sinning, A., & Luhmann, H. J. (2017). Electrical activity controls area-specific expression of neuronal apoptosis in the mouse developing cerebral cortex. *ELife*, *6*. https://doi.org/10.7554/eLife.27696

Bramley, J. R., Wiles, E. M., Sollars, P. J., & Pickard, G. E. (2011). Carbenoxolone blocks the light-evoked rise in intracellular calcium in isolated melanopsin ganglion cell photoreceptors. *PloS One*, *6*(7), e22721. https://doi.org/10.1371/journal.pone.0022721

Braunger, B. M., Demmer, C., & Tamm, E. R. (2014). Programmed cell death during retinal development of the mouse eye. *Advances in Experimental Medicine and Biology*, *801*, 9–13. https://doi.org/10.1007/978-1-4614-3209-8_2

Burbridge, T. J., Xu, H. P., Ackman, J. B., Ge, X., Zhang, Y., Ye, M. J., Zhou, Z. J., Xu, J., Contractor, A., & Crair, M. C. (2014). Visual circuit development requires patterned activity mediated by retinal acetylcholine receptors. *Neuron*, *84*(5), 1049–1064. https://doi.org/10.1016/j.neuron.2014.10.051

Catsicas, M., Bonness, V., Becker, D., & Mobbs, P. (1998). Spontaneous Ca2+ transients and their transmission in the developing chick retina. *Current Biology*, *8*(5), 283–288. https://doi.org/10.1016/s0960-9822(98)70110-1

Caval-Holme, F., & Feller, M. B. (2019). Gap Junction Coupling Shapes the Encoding of Light in the Developing Retina. *Current Biology*, *29*(23), 4024-4035.e5. https://doi.org/10.1016/j.cub.2019.10.025

Caval-Holme, F., Aranda, M. L., Chen, A. Q., Tiriac, A., Zhang, Y., Smith, B., Birnbaumer, L., Schmidt, T. M., & Feller, M. B. (2022). The Retinal Basis of Light Aversion in Neonatal Mice. *The Journal of Neuroscience*, *42*(20), 4101–4115. https://doi.org/10.1523/JNEUROSCI.0151-22.2022

Cepko, C. (2014). Intrinsically different retinal progenitor cells produce specific types of progeny. In *Nature Reviews Neuroscience* (Vol. 15, Issue 9, pp. 615–627). Nature Publishing Group. https://doi.org/10.1038/nrn3767

Chakraborty, R., Landis, E. G., Mazade, R., Yang, V., Strickland, R., Hattar, S., Stone, R. A., Iuvone, P. M., & Pardue, M. T. (2022). Melanopsin modulates refractive development and

myopia. *Experimental Eye Research*, *214*. https://doi.org/10.1016/J.EXER.2021.108866

Chen, S. K., Chew, K. S., McNeill, D. S., Keeley, P. W., Ecker, J. L., Mao, B. Q., Pahlberg, J., Kim, B., Lee, S. C. S., Fox, M. A., Guido, W., Wong, K. Y., Sampath, A. P., Reese, B. E., Kuruvilla, R., & Hattar, S. (2013). Apoptosis Regulates ipRGC Spacing Necessary for Rods and Cones to Drive Circadian Photoentrainment. *Neuron*, *77*(3), 503–515. https://doi.org/10.1016/j.neuron.2012.11.028

Chew, K. S., Renna, J. M., McNeill, D. S., Fernandez, D. C., Keenan, W. T., Thomsen, M. B., Ecker, J. L., Loevinsohn, G. S., Vandunk, C., Vicarel, D. C., Tufford, A., Weng, S., Gray, P. A., Cayouette, M., Herzog, E. D., Zhao, H., Berson, D. M., & Hattar, S. (2017). A subset of iprgcs regulates both maturation of the circadian clock and segregation of retinogeniculate projections in mice. *ELife*, *6*. https://doi.org/10.7554/eLife.22861

Choi, B. J., Chen, Y. C. D., & Desplan, C. (2021). Building a circuit through correlated spontaneous neuronal activity in the developing vertebrate and invertebrate visual systems. In *Genes and Development* (Vol. 35, Issues 9–10, pp. 677–691). Cold Spring Harbor Laboratory Press. https://doi.org/10.1101/GAD.348241.121

Cook, J. E., & Becker, D. L. (2009). Gap-junction proteins in retinal development: new roles for the “nexus.” In *Physiology* (Vol. 24, Issue 4, pp. 219–230). Physiology (Bethesda). https://doi.org/10.1152/physiol.00007.2009

Corrie, L. W., Stokes, C., Wilkerson, J. L., Carroll, F. I., Mcmahon, L. R., & Papke, R. L. (2020). Nicotinic Acetylcholine Receptor Accessory Subunits Determine the Activity Profile of Epibatidine Derivatives s. *MOLECULAR PHARMACOLOGY Mol Pharmacol*, *98*, 328–342. https://doi.org/10.1124/molpharm.120.000037

Ecker, J. L., Dumitrescu, O. N., Wong, K. Y., Alam, N. M., Chen, S. K., LeGates, T., Renna, J. M., Prusky, G. T., Berson, D. M., & Hattar, S. (2010). Melanopsin-expressing retinal ganglion-cell photoreceptors: Cellular diversity and role in pattern vision. *Neuron*, *67*(1), 49–60. https://doi.org/10.1016/j.neuron.2010.05.023

Emanuel, A. J., & Do, M. T. H. (2015). Melanopsin tristability for sustained and broadband phototransduction. *Neuron*, *85*(5), 1043–1055. https://doi.org/10.1016/j.neuron.2015.02.011

Feller, M. B., Butts, D. A., Aaron, H. L., Rokhsar, D. S., & Shatz, C. J. (1997). Dynamic processes shape spatiotemporal properties of retinal waves. *Neuron*, *19*(2). https://doi.org/10.1016/S0896-6273(00)80940-X

Feller, M. B., & Kerschensteiner, D. (2013). Retinal Waves and their Role in Visual System Development. *Cellular Migration and Formation of Neuronal Connections*, *2*, 941–953. https://doi.org/10.1016/B978-0-12-397266-8.00042-9

Ford, K.J., & Feller, M. B. (2012). Assembly and disassembly of a retinal cholinergic network. *Visual Neuroscience*, *29*(1). https://doi.org/10.1017/S0952523811000216

Ford, K.J., Félix, A. L., & Feller, M. B. (2012). *Cellular Mechanisms Underlying*

Spatiotemporal Features of Cholinergic Retinal Waves. https://doi.org/10.1523/JNEUROSCI.5309-12.2012

Fujimoto, S., Leiwe, M. N., Sakaguchi, R., Muroyama, Y., Kobayakawa, R., Kobayakawa, K., Saito, T., & Imai, T. (2019). Spontaneous activity generated within the olfactory bulb establishes the discrete wiring of mitral cell dendrites. *BioRxiv*, 625616. https://doi.org/10.1101/625616

Ge, X., Zhang, K., Gribizis, A., Hamodi, A. S., Sabino, A. M., & Crair, M. C. (2021). Retinal waves prime visual motion detection by simulating future optic flow. *Science*, *373*(6553). https://doi.org/10.1126/science.abd0830

Goldberg, J. L., Espinosa, J. S., Xu, Y., Davidson, N., Kovacs, G. T. A., & Barres, B. A. (2002). Retinal ganglion cells do not extend axons by default: Promotion by neurotrophic signaling and electrical activity. *Neuron*, *33*(5), 689–702. https://doi.org/10.1016/S0896-6273(02)00602-5

Grubb, M. S., Rossi, F. M., Changeux, J. P., & Thompson, I. D. (2003). Abnormal functional organization in the dorsal lateral geniculate nucleus of mice lacking the β2 subunit of the nicotinic acetylcholine receptor. *Neuron*, *40*(6), 1161–1172. https://doi.org/10.1016/S0896-6273(03)00789-X

Harvey, S. C., & Luetje, C. W. (1996). Determinants of competitive antagonist sensitivity on neuronal nicotinic receptor β subunits. *Journal of Neuroscience*, *16*(12), 3798–3806. https://doi.org/10.1523/jneurosci.16-12-03798.1996

Harvey, S. C., Maddox, F. N., & Luetje, C. W. (1996). Multiple determinants of dihydro-beta-erythroidine sensitivity on rat neuronal nicotinic receptor alpha subunits. *Journal of Neurochemistry*, *67*(5), 1953–1959. https://doi.org/10.1046/J.1471-4159.1996.67051953.X

Hilgen, G., Pirmoradian, S., Pamplona, D., Kornprobst, P., Cessac, B., Hennig, M. H., & Sernagor, E. (2017). Pan-retinal characterisation of Light Responses from Ganglion Cells in the Developing Mouse Retina. *Scientific Reports 2017 7:1*, *7*(1), 1–14. https://doi.org/10.1038/srep42330

Ho, T. N. T., Abraham, N., & Lewis, R. J. (2020). Structure-Function of Neuronal Nicotinic Acetylcholine Receptor Inhibitors Derived From Natural Toxins. In *Frontiers in Neuroscience* (Vol. 14). Frontiers Media S.A. https://doi.org/10.3389/fnins.2020.609005

Hoon, M., Okawa, H., Della Santina, L., & Wong, R. O. L. (2014). Functional architecture of the retina: development and disease. *Progress in Retinal and Eye Research*, *42*, 44–84. https://doi.org/10.1016/j.preteyeres.2014.06.003

Kähne, M., Rüdiger, S., Kihara, A. H., & Lindner, B. (2019). Gap junctions set the speed and nucleation rate of stage I retinal waves. *PLoS Computational Biology*, *15*(4), 1–15. https://doi.org/10.1371/journal.pcbi.1006355

Keeley, P. W., Eglen, S. J., & Reese, B. E. (2020). From random to regular: Variation in the

patterning of retinal mosaics*. In *Journal of Comparative Neurology* (Vol. 528, Issue 13, pp. 2135–2160). Wiley-Liss Inc. https://doi.org/10.1002/cne.24880

Kim, I. B., Lee, E. J., Kim, M. K., Park, D. K., & Chun, M. H. (2000). Choline acetyltransferase-immunoreactive neurons in the developing rat retina. *Journal of Comparative Neurology*, *427*(4), 604–616. https://doi.org/10.1002/1096-9861(20001127)427:4<604::AID-CNE8>3.0.CO;2-C

Kirkby, L.A., & Feller, M. B. (2013). Intrinsically photosensitive ganglion cells contribute to plasticity in retinal wave circuits. *Proceedings of the National Academy of Sciences of the United States of America*, *110*(29). https://doi.org/10.1073/pnas.1222150110

Kirkby, L.A., Sack, G. S., Firl, A., & Feller, M. B. (2013). A role for correlated spontaneous activity in the assembly of neural circuits. *Neuron*, *80*(5), 1129–1144. https://doi.org/10.1016/j.neuron.2013.10.030

Kuo, S. P., Schwartz, G. W., & Rieke, F. (2016). Nonlinear Spatiotemporal Integration by Electrical and Chemical Synapses in the Retina. *Neuron*, *90*(2), 320–332. https://doi.org/10.1016/j.neuron.2016.03.012

Legland, D., Arganda-Carreras, I., & Andrey, P. (2016). MorphoLibJ: integrated library and plugins for mathematical morphology with ImageJ. *Bioinformatics*, *32*(22), btw413. https://doi.org/10.1093/bioinformatics/btw413

Lucas, J. A., & Schmidt, T. M. (2019). Cellular properties of intrinsically photosensitive retinal ganglion cells during postnatal development. *Neural Development*, *14*(1), 1–19. https://doi.org/10.1186/s13064-019-0132-2

Luhmann, H. J., & Khazipov, R. (2018). Neuronal activity patterns in the developing barrel cortex. *Neuroscience*, *368*, 256–267. https://doi.org/10.1016/j.neuroscience.2017.05.025

Spontaneous activity in developing thalamic and cortical sensory networks, 109 Neuron 2519 (2021).

McNeill, D. S., Sheely, C. J., Ecker, J. L., Badea, T. C., Morhardt, D., Guido, W., & Hattar, S. (2011). Development of melanopsin-based irradiance detecting circuitry. *Neural Development*, *6*(1), 2–11. https://doi.org/10.1186/1749-8104-6-8

Moreno-Juan, V., Aníbal-Martínez, M., Herrero-Navarro, Á., Valdeolmillos, M., Martini, F. J., & López-Bendito, G. (2022). Spontaneous Thalamic Activity Modulates the Cortical Innervation of the Primary Visual Nucleus of the Thalamus. *Neuroscience*. https://doi.org/10.1016/j.neuroscience.2022.07.022

Pan, F., Mills, S. L., & Massey, S. C. (2007). Screening of gap junction antagonists on dye coupling in the rabbit retina. *Visual Neuroscience*, *24*(04), 609–618. https://doi.org/10.1017/S0952523807070472

Papke, R. L., Wecker, L., & Stitzel, J. A. (2010). Activation and inhibition of mouse muscle and

neuronal nicotinic acetylcholine receptors expressed in xenopus oocytes. *Journal of Pharmacology and Experimental Therapeutics*, *333*(2), 501–518. https://doi.org/10.1124/jpet.109.164566

Rao, S., Chun, C., Fan, J., Kofron, J. M., Yang, M. B., Hegde, R. S., Ferrara, N., Copenhagen, D. R., & Lang, R. A. (2013). A direct and melanopsin-dependent fetal light response regulates mouse eye development. *Nature*, *494*(7436), 243–246. https://doi.org/10.1038/nature11823

Ray, T. A., Roy, S., Kozlowski, C., Wang, J., Cafaro, J., Hulbert, S. W., Wright, C. V, Field, G. D., & Kay, J. N. (2018). Formation of retinal direction-selective circuitry initiated by starburst amacrine cell homotypic contact. *ELife*, 1–44. doi: https://doi.org/10.7554/eLife.34241

Rossi, F. M., Pizzorusso, T., Porciatti, V., Marubio, L. M., Maffei, L., & Changeux, J. P. (2001). Requirement of the nicotinic acetylcholine receptor beta 2 subunit for the anatomical and functional development of the visual system. *Proceedings of the National Academy of Sciences of the United States of America*, *98*(11), 6453–6458. https://doi.org/10.1073/PNAS.101120998

Schneider, B. F., & Norton, S. (1979). Equivalent ages in rat, mouse and chick embryos. *Teratology*, *19*(3), 273–278. https://doi.org/10.1002/tera.1420190302

Shekhar, K., Whitney, I. E., Butrus, S., Peng, Y.-R., & Sanes, J. R. (2022). Diversification of multipotential postmitotic mouse retinal ganglion cell precursors into discrete types. *ELife*, *11*. https://doi.org/10.7554/eLife.73809

Singer, J. H., Mirotznik, R. R., & Feller, M. B. (2001). Potentiation of L-type calcium channels reveals nonsynaptic mechanisms that correlate spontaneous activity in the developing mammalian retina. *The Journal of Neuroscience : The Official Journal of the Society for Neuroscience*, *21*(21), 8514–8522. http://www.ncbi.nlm.nih.gov/pubmed/11606640

Spang, J. E., Bertrand, S., Westera, G., Patt, J. T., Schubiger, P. A., & Bertrand, D. (2000). Chemical modification of epibatidine causes a switch from agonist to antagonist and modifies its selectivity for neuronal nicotinic acetylcholine receptors. *Chemistry and Biology*, *7*(7), 545–555. https://doi.org/10.1016/S1074-5521(00)00138-1

Spirova, E. N., Ivanov, I. A., Kasheverov, I. E., Kudryavtsev, D. S., Shelukhina, I. V., Garifulina, A. I., Son, L. V., Lummis, S. C. R., Malca-Garcia, G. R., Bussmann, R. W., Hennig, L., Giannis, A., & Tsetlin, V. I. (2019). Curare alkaloids from matis dart poison: Comparison with d-tubocurarine in interactions with nicotinic, 5-HT 3 serotonin and GABA A receptors. *PLoS ONE*, *14*(1). https://doi.org/10.1371/journal.pone.0210182

Stafford, B. K., Sher, A., Litke, A. M., & Feldheim, D. A. (2009). Spatial-Temporal Patterns of Retinal Waves Underlying Activity-Dependent Refinement of Retinofugal Projections. *Neuron*, *64*(2), 200–212. https://doi.org/10.1016/j.neuron.2009.09.021

Syed, M. M., Lee, S., Zheng, J., & Zhou, Z. J. (2004). Stage-dependent dynamics and modulation of spontaneous waves in the developing rabbit retina. *Journal of Physiology*,

560(2), 533–549. https://doi.org/10.1113/jphysiol.2004.066597

Thompson, A., Gribizis, A., Chen, C., & Crair, M. C. (2017). Activity-dependent development of visual receptive fields. *Current Opinion in Neurobiology*, *42*, 136–143. https://doi.org/10.1016/j.conb.2016.12.007

Tiriac, A., Bistrong, K., Pitcher, M. N., Tworig, J. M., & Feller, M. B. (2022). *The influence of spontaneous and visual activity on the development of direction selectivity maps in mouse retina*. *38*(2).

Tiriac, A., Smith, B. E., & Feller, M. B. (2018). Light Prior to Eye Opening Promotes Retinal Waves and Eye-Specific Segregation. *Neuron*, *100*(5), 1059-1065.e4. https://doi.org/10.1016/J.NEURON.2018.10.011

Torborg, C. L., Hansen, K. A., & Feller, M. B. (2005). High frequency, synchronized bursting drives eye-specific segregation of retinogeniculate projections. *Nature Neuroscience*, *8*(1). https://doi.org/10.1038/nn1376

Veruki, M. L., & Hartveit, E. (2009). Meclofenamic Acid Blocks Electrical Synapses of Retinal AII Amacrine and on -Cone Bipolar Cells. *Journal of Neurophysiology*, *101*(5), 2339–2347. https://doi.org/10.1152/jn.00112.2009

Verweij, J., Chaney, S., Bredl, D., Vemaraju, S., König, G., Kostenis, E., Lang, R., & Copenhagen, D. (2019). Light responses of melanopsin-expressing ganglion cells in the foetal mammalian retina. *BiorX*, *7351*, 675702. https://doi.org/10.1101/675702

Wang, L., Rangarajan, K. V., Lawhn-Heath, C. A., Sarnaik, R., Wang, B. S., Liu, X., & Cang, J. (2009). Direction-specific disruption of subcortical visual behavior and receptive fields in mice lacking the β2 subunit of nicotinic acetylcholine receptor. *Journal of Neuroscience*, *29*(41), 12909–12918. https://doi.org/10.1523/JNEUROSCI.2128-09.2009

Weiner, G. A., Shah, S. H., Angelopoulos, C. M., Bartakova, A. B., Pulido, R. S., Murphy, A., Nudleman, E., Daneman, R., & Goldberg, J. L. (2019). Cholinergic neural activity directs retinal layer-specific angiogenesis and blood retinal barrier formation. *Nature Communications*, *10*(1). https://doi.org/10.1038/s41467-019-10219-8

Whitney, I. E., Butrus, S., Dyer, M. A., Rieke, F., Sanes, J. R., & Shekhar, K. (2022). Vision-Dependent and -Independent Molecular Maturation of Mouse Retinal Ganglion Cells. *Neuroscience*. https://doi.org/10.1016/j.neuroscience.2022.07.013

Wong, R. O. L. (1999). Retinal waves: stirring up a storm. *Neuron*, *24*(3), 493–495.

Wong, R. O. L. (1995). Cholinergic regulation of [Ca2+](i) during cell division and differentiation in the mammalian retina. *Journal of Neuroscience*, *15*(4), 2696–2706. https://doi.org/10.1523/jneurosci.15-04-02696.1995

Wong, W. T., Sanes, J. R., & Wong, R. O. L. (1998). Developmentally regulated spontaneous activity in the embryonic chick retina. *Journal of Neuroscience*, *18*(21), 8839–8852.

https://doi.org/10.1523/jneurosci.18-21-08839.1998

Wotring, V. E., & Yoon, K. W. (1995). The inhibitory effects of nicotinic antagonists on currents elicited by GABA in rat hippocampal neurons. *Neuroscience*, *67*(2), 293–300. https://doi.org/10.1016/0306-4522(95)00011-7

Xu, H. P., Burbridge, T. J., Chen, M. G., Ge, X., Zhang, Y., Zhou, Z. J., & Crair, M. C. (2015). Spatial pattern of spontaneous retinal waves instructs retinotopic map refinement more than activity frequency. *Developmental Neurobiology*, *75*(6), 621–640. https://doi.org/10.1002/dneu.22288

Xu, H. P., Burbridge, T. J., Ye, M., Chen, M., Ge, X., Zhou, Z. J., & Crair, M. C. (2016). Retinal wave patterns are governed by mutual excitation among starburst amacrine cells and drive the refinement and maintenance of visual circuits. *Journal of Neuroscience*, *36*(13), 3871–3886. https://doi.org/10.1523/JNEUROSCI.3549-15.2016

Xu, W., Orr-Urtreger, A., Nigro, F., Gelber, S., Sutcliffe, C. B., Armstrong, D., Patrick, J. W., Role, L. W., Beaudet, A. L., & De Biasi, M. (1999). Multiorgan autonomic dysfunction in mice lacking the β2 and the β4 subunits of neuronal nicotinic acetylcholine receptors. *Journal of Neuroscience*, *19*(21), 9298–9305. https://doi.org/10.1523/jneurosci.19-21-09298.1999

Young, R. W. (1984). Cell death during differentiation of the retina in the mouse. *Journal of Comparative Neurology*, *229*(3), 362–373. https://doi.org/10.1002/cne.902290307

TABLES

Table 1: Stage 1 wave speeds in WT and β2-nAChR-KO, plus Stage 2 wave speeds

	WT Stage 1 waves velocity	β2 KO Stage 1 waves velocity
	174.1658075	77.90558644
	183.9436667	92.40253599
	192.190149	98.1860635
	162.2612779	117.3380651
	189.8368251	128.5237364
	237.3368694	87.97212726
	179.2431575	92.40411967
	165.6813312	92.06444749
	144.5218287	103.246318
	182.0663497	103.8986282
	135.9836566	134.1626649
	164.1422662	146.1075903
	177.7751553	203.6008266
	197.1502675	88.47319817
	163.5210281	124.1823287
	192.5917948	156.7712906
	156.152095	135.6789987
	199.893442	185.0688707
	186.1464734	197.5310269
	179.7713095	101.5179598
	181.4363548	158.4677627
	202.2187698	121.8116385
	136.1837197	140.1408581
	178.1366311	224.9681719
	166.4619956	172.2776595
	239.4060251	165.4374183
	277.753129	177.693694
	212.8923028	135.5548662
	302.3533818	174.3332815
	241.7414928	138.9493641
Avg	**190.0986185**	**135.8890366**
SD	**37.95551205**	**39.07396588**

Summary data (μm/sec) reported in Figure 3. Each row is an individual wave.

Table 2: Nearest-neighbor distances and regularity indices for ipRGCs labeled in Opn4cre::Td-tomato mice

	Median nearest neighbor distance (µm)	Regularity Index (NND/SD)	Number of retinas
WT P1	11.59± 0.93	2.83±0.12	9
β2 P1	11.51±0.55	2.89 ±0.16	9
WT P7	22.32±0.58	2.33±0.13	8
β2 P7	20.96±1.40	2.55±0.20	8

Summary data reported in Figure 5. Data represented as averages ± SD.

Table 3: Density of tdTom+ cells per quadrant

Density per quadrant per retina										
P1						**P7**				
	DN	**DT**	**VN**	**VT**			**DN**	**DT**	**VN**	**VT**
OCTP1211021M1L	37	24	33	33		OCTP1220222M1R	36	64	35	55
OCTP1211021M1R	33	21	24	28		OCTP1220222M2L	57	43	51	52
OCTP1211021M3L	31	19	29	26		OCTP1220222M3L	48	48	56	63
OCTP1211021M3R	25	30	19	29		OCTP1220222M4R	56	42	49	52
OCTP1220125M1R	15	24	24	20		OCTP1220222M5R	40	34	56	39
OCTP1220125M2R	29	22	20	32		OCTP1220222M6L	52	47	42	43
OCTP1220125M3L	30	26	19	20		OCTP1220222M7L	35	54	56	53
OCTP1220125M4L	21	26	25	30		OCTP1220222M8R	46	36	54	61
OCTP1220125M4R	28	16	28	28						
Average	**27.67**	**23.11**	**24.56**	**27.33**		**Average**	**46.25**	**46**	**49.88**	**52.25**
Std	**6.58**	**4.17**	**4.82**	**4.66**		**Std**	**8.6**	**9.72**	**7.7**	**8.12**
	DN	**DT**	**VN**	**VT**						
BTOTP1220108M3L	25	28	24	22			**DN**	**DT**	**VN**	**VT**
BTOTP1220124M1L	18	9	12	17		BTOTP1211004M1R	36	25	33	32
BTOTP1220124M1R	19	31	21	28		BTOTP1211004M2L	39	43	38	49
BTOTP1220124M2L	15	21	21	31		BTOTP1211004M2R	37	34	39	30
BTOTP1220124M3L	29	14	26	23		BTOTP1220222M1R	43	39	40	46
BTOTP1220209M2R	32	21	23	18		BTOTP1220222M2L	48	38	57	72
BTOTP1220209M3R	25	25	30	23		BTOTP1220222M2R	49	40	44	58
BTOTP1220209M4L	20	22	27	15		BTOTP1220222M3L	48	38	57	38
BTOTP1220209M4R	29	27	22	29		BTOTP1220222M3R	38	40	44	40
Average	**23.56**	**22**	**22.89**	**22.89**		**Average**	**42.25**	**37.13**	**44**	**45.63**
Std	**5.83**	**6.95**	**5.06**	**5.6**		**Std**	**5.44**	**5.51**	**8.75**	**14.04**

Summary data reported in Figure 5. Each row is a retina. No significant difference in density across quadrants.

FIGURES

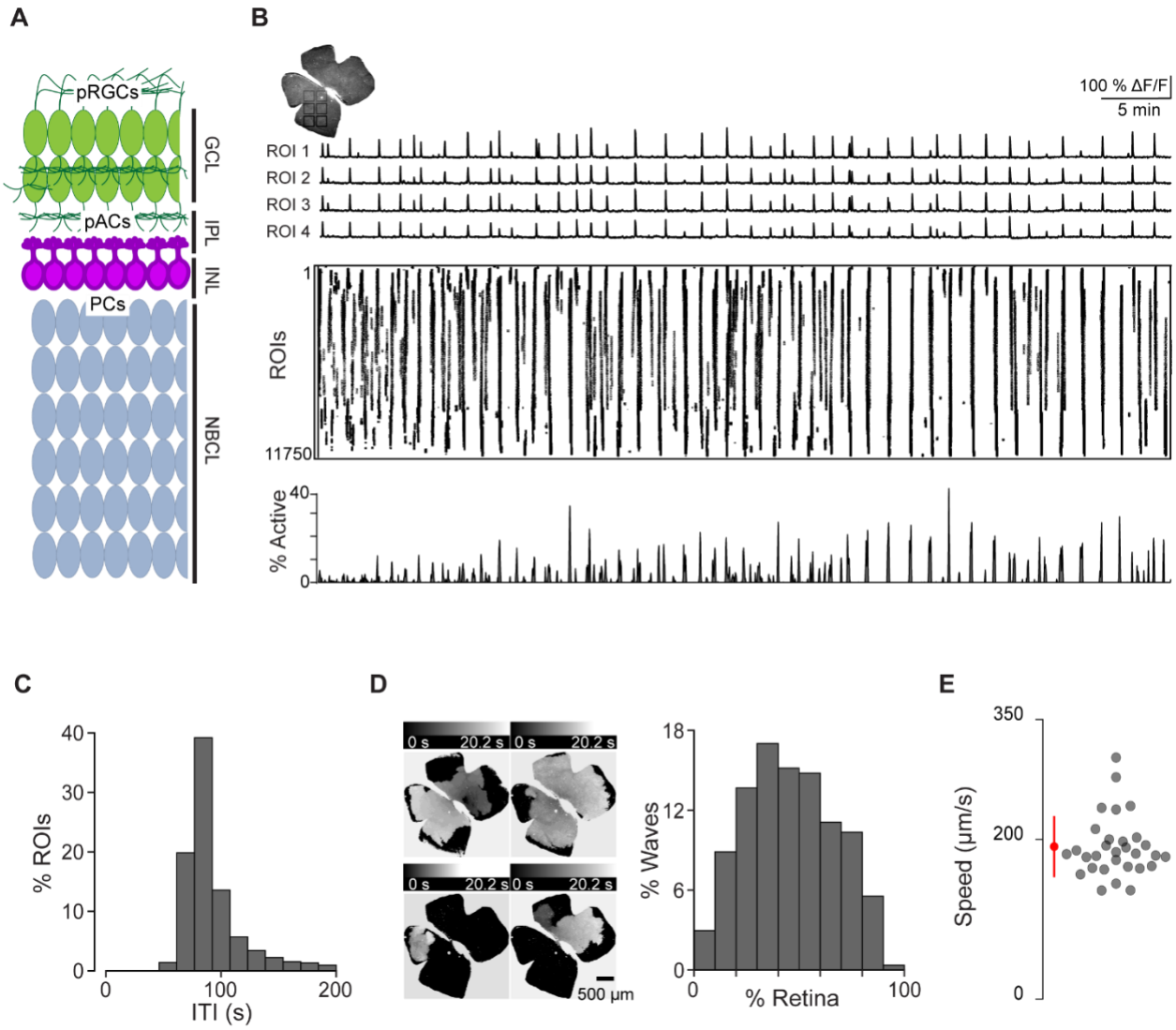

Figure 1. Spatiotemporal characteristics of embryonic waves. A, schematized cross section of an E16 retina when Stage 1 waves begin. Green cells represent post-mitotic retinal ganglion cells (pRGCs). Magenta cells represent post-mitotic amacrine cells (pACs). Gray cells, represent progenitor cells and proliferating cells (PCs). GCL, ganglion cell layer; IPL, inner plexiform layer; INL, inner nuclear layer; NBCL, neuroblastic cell layer. **B,** top left: Macroscope image of the baseline fluorescence of an E17 GCaMP6s retina. For subsequent analysis, the retina was divided into 11,750 10 µm x 10 µm (not drawn to scale) squares. Number of ROIs changed depending on retina size. Top: ΔF/F traces of calcium transients from four example 10 µm x 10 µm ROIs. Middle: rasterized calcium transients for all ROIs raster plot of calcium transients > 50% ΔF/F . Bottom: Percentage of ROIs active throughout the time course of the recording (1

hour). **C**, Histogram showing the distribution of the percent of ROIs with inter-transient-intervals (ITIs) ranging from 0 - 200s. **D**, Left: heatmap showing the temporal progression and spread of 4 example waves observed with epifluorescent calcium imaging on the macroscope. Scale depicts timescale of propagation, dark gray = start of propagation and white = end of propagation. Right: Histogram showing the distribution of waves with an area ranging from 0-100% of the retina. **E**, Summary plot of wave speeds. n = 30 waves, 3 retinas, 3 mice.

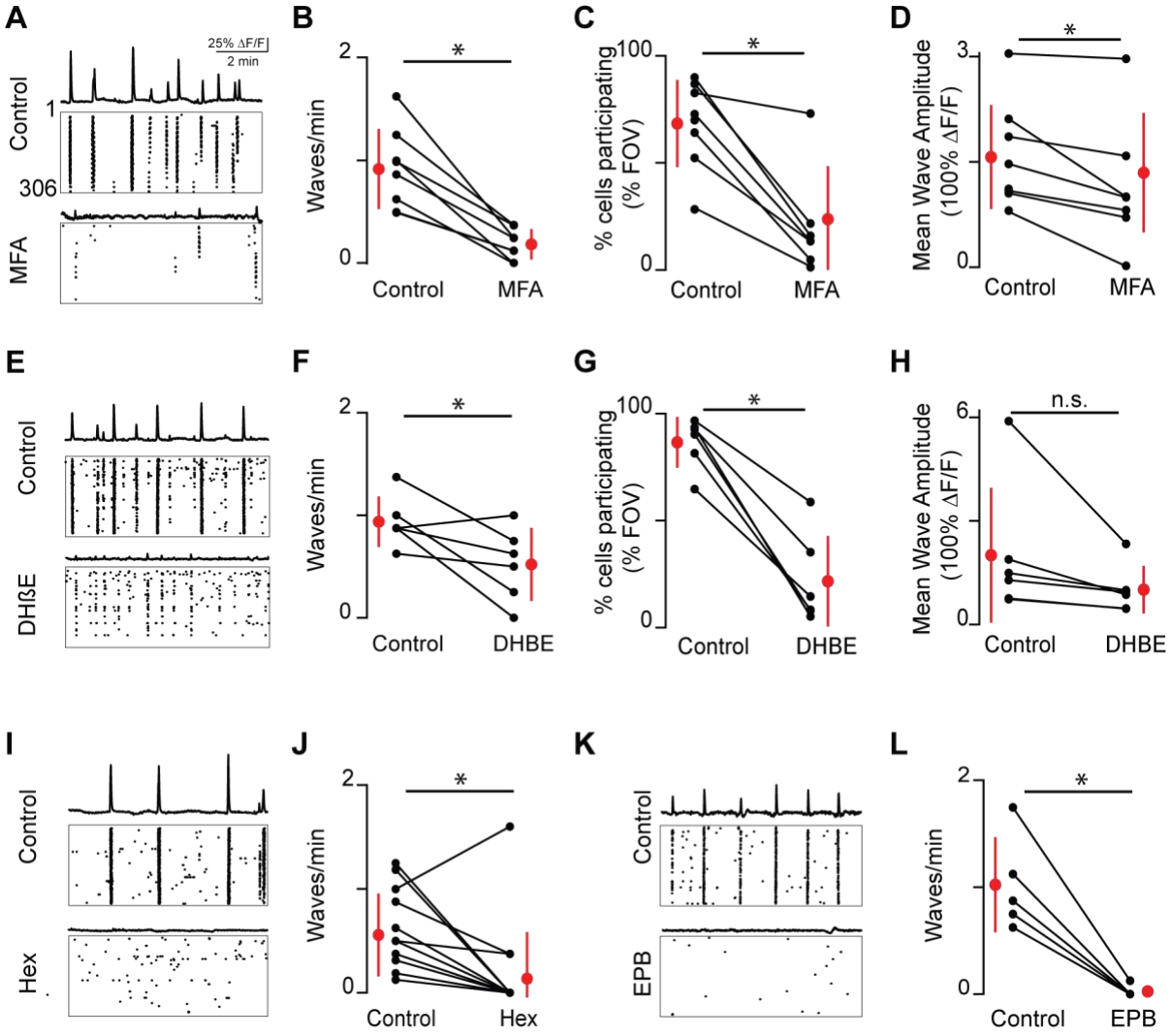

Figure 2. Embryonic waves are mediated by gap junction and cholinergic circuits.

A: ΔF/F time course of spontaneous activity observed in the field of view (FOV) and raster plot of neuronal calcium transients in ACSF (control condition, top) and in the presence of MFA (bottom).

B : Summary plot showing frequency of waves in control and MFA. Red dots and lines = mean and standard deviation, respectively. Asterisks represents significant effects. n = 8 retinas (6 mice); $p = 4.81e^{-4}$

C. Percent cells that participate in retinal waves in control and MFA ($p = 3e^{-3}$);

D. Mean calcium response of the neurons that participate in waves in control and MFA (p = 0.02).

E-H: Same as A-D for dihydro-β-erythroidine (DhβE, 8 µM). (n = 6 retinas; 6 mice); F: p = 0.05; G: $p = 4.58e^{-4}$; H: p= 0.09)

I-J Same as A-B but with Hexamethonium (Hex, 100 µM) following a baseline recording. n = 14 retinas (9 mice); $p = 1.48^{-2}$.

K-L Same as A but with epibatidine (EPB, 10 nM) following a baseline recording. n = 5 retinas (5 mice); p = $4.8e^{-3}$.
DhβE (Left, n = 6 retinas (6 mice); p = 0.09) or
Percent cells that participate in retinal waves in control and DhβE (p = $3e^{-3}$); RIGHT: Mean calcium response of the neurons that participate in waves in control and DhβE (Left, n = 6 retinas (6 mice); p = 0.09) or MFA (Right, n = 8 retinas (6 mice); p = 0.02).

B, Same as A but with dihydro-β-erythroidine (DhβE, 8 μM). n = 6 retinas (6 mice); p = 0.05. **C**, C. Same as A but with Hexamethonium (Hex, 100 μM) following a baseline recording. n = 14 retinas (9 mice); p = 1.48^{-2}. **D**, Same as A but with epibatidine (EPB, 10 nM) following a baseline recording. n = 5 retinas (5 mice); p = $4.8e^{-3}$. **RIGHT MIDDLE**, Percent cells that participate in retinal waves in control and DhβE (Left, n = 6 retinas (6 mice); p = $4.58e^{-4}$) or MFA (Right, n = 8 retinas (6 mice); p = $3e^{-3}$). **F**, Mean calcium response of the neurons that participate in waves in control and DhβE (Left, n = 6 retinas (6 mice); p = 0.09) or MFA (Right, n = 8 retinas (6 mice); p = 0.02). All statistical tests here are paired t-tests.

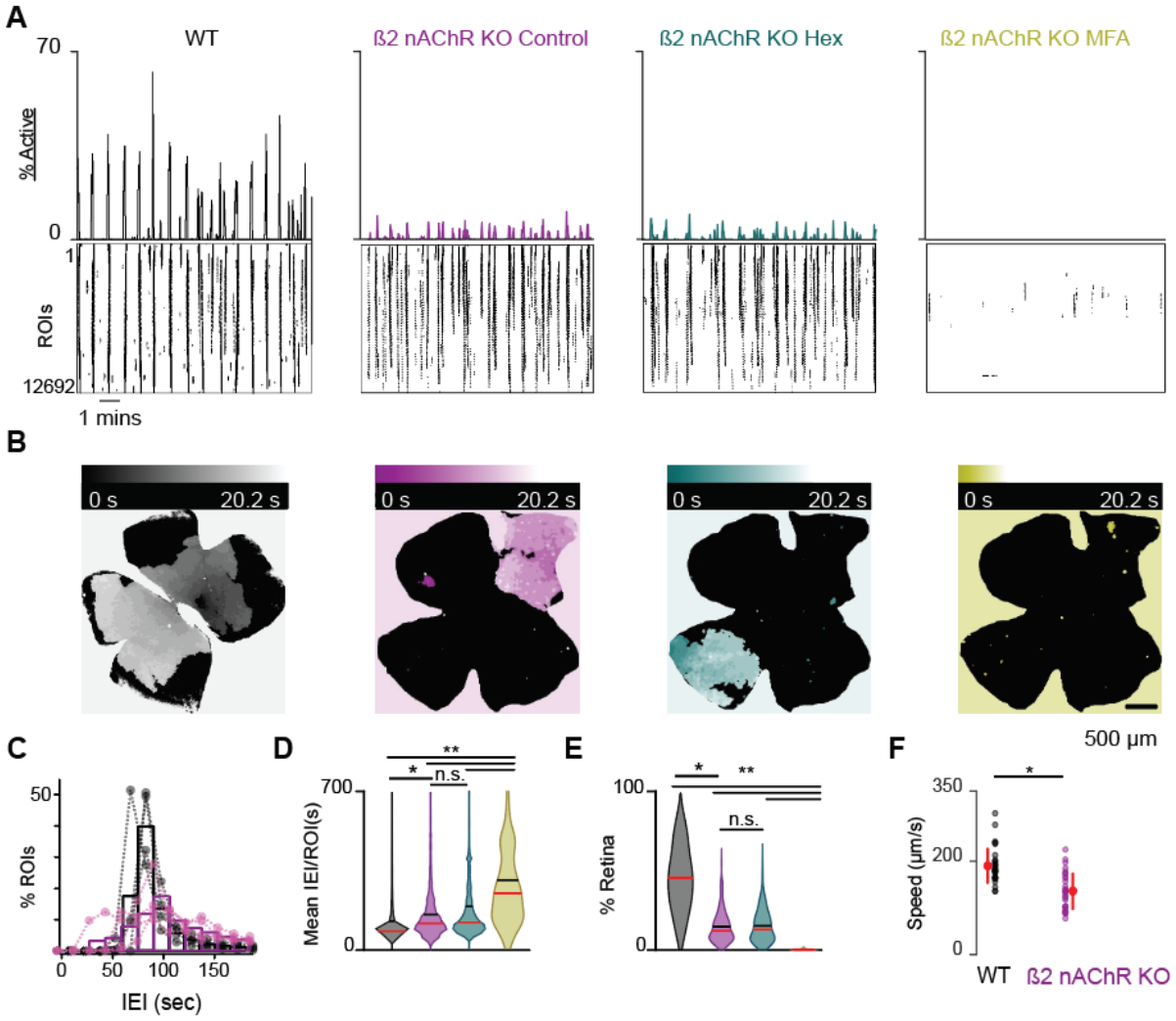

Figure 3. β2-nAChR-KO mice have reduced stage 1 wave activity. A, top, area plot summarizing the percentage of ROIs active throughout the time course of the recording; bottom, raster plots of ROI calcium transients across conditions. Black: WT control; magenta: β2-nAChR-KO control; teal: β2-nAChR-KO in Hex; yellow: β2-nAChR-KO in MFA. **B**, heatmap showing the temporal progression of a propagating wave observed using epifluorescent calcium imaging on the macroscope across experimental conditions. Scale depicts timescale of propagation, dark colors = start of propagation and white = end of propagation. **C,** mean IEI/ ROI in WT and β2-nAChR-KO retinas in control conditions. Black bar = mean; red bar = median. **D & E**, violin plots summarizing the distribution of mean ITI/ ROI (D) and wave area (E) across experimental conditions. n = 4 retinas, 4 mice (WT), n = 5 retinas, 5 mice (β2-nAChR-KO) (**D** & **E**); **p < 0.01. One-way ANOVA, followed by Tukey-Kramer post hoc test (right); Kruskal-Wallis, followed by Dunn-Sidak post hoc test (left). **F**, summary plot of wave

speed in WT and β2-nAChR-KO retinas in control conditions. n = 30 waves, 3 retinas, 3 mice per condition; p = 1.19e^{-6}. Unpaired t-test.

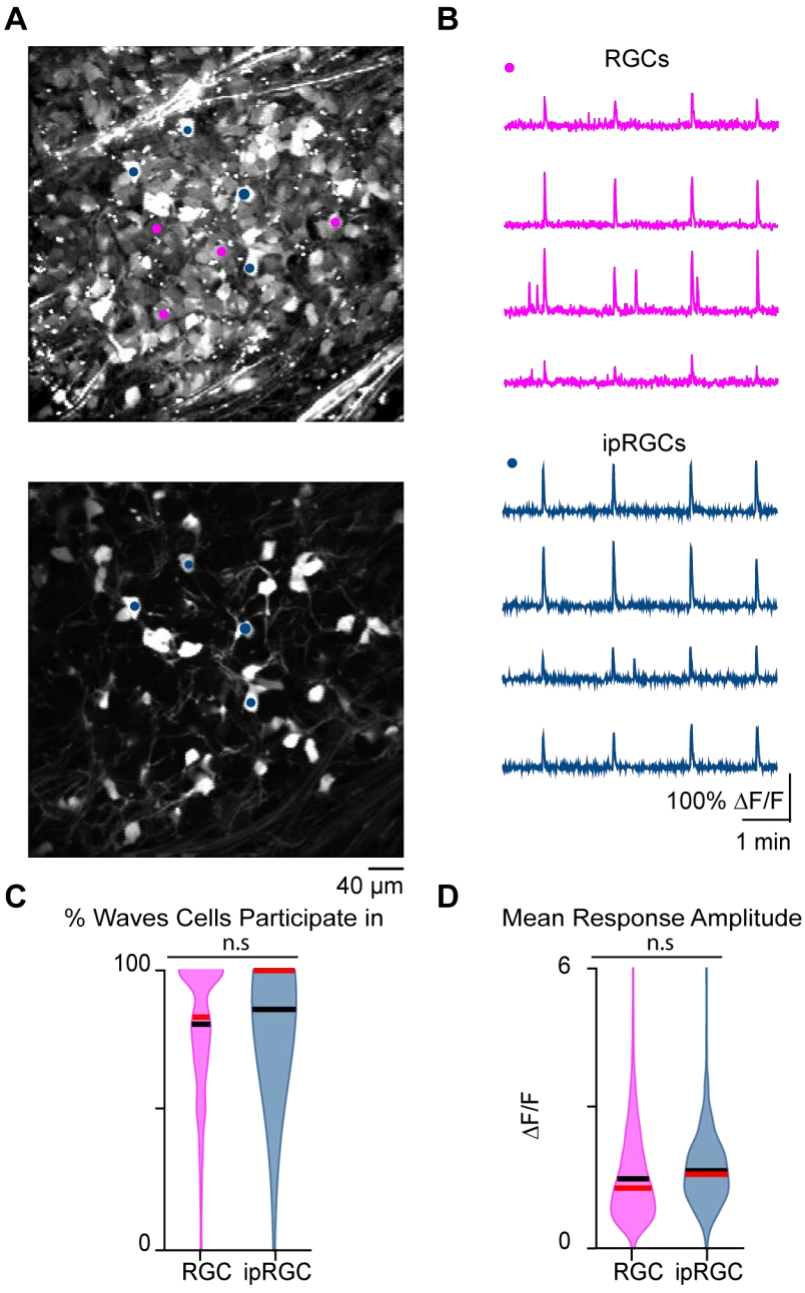

Figure 4. Stage 1 waves robustly recruit ipRGCs and the general RGC population. A. *Top:* Example FOV where pixel intensity was averaged across all frames (712) to get representative image of Cal 520 bath loaded RGCs. Pink dots correspond to four example RGCs and blue dots correspond to four example ipRGCs *Bottom:* same example FOV from the top image, with tdTom signal averaged across all frames. Blue dots the same as those in the top image. **B**. *Top:* traces of the four example RGCs marked by the pink circles in **A**. *Bottom:* traces of four example ipRGCs marked by the blue circles in **A**. **C**. Violin plot of percentage of waves each cell participated in. n = 20 retinas (13 mice); p = 0.09. Unpaired t-test. **D**. Violin plot of mean wave amplitude/cell/FOV. n = 20 retinas (13 mice); p = 0.06. Unpaired t-test. Black bar = mean; red bar = median.

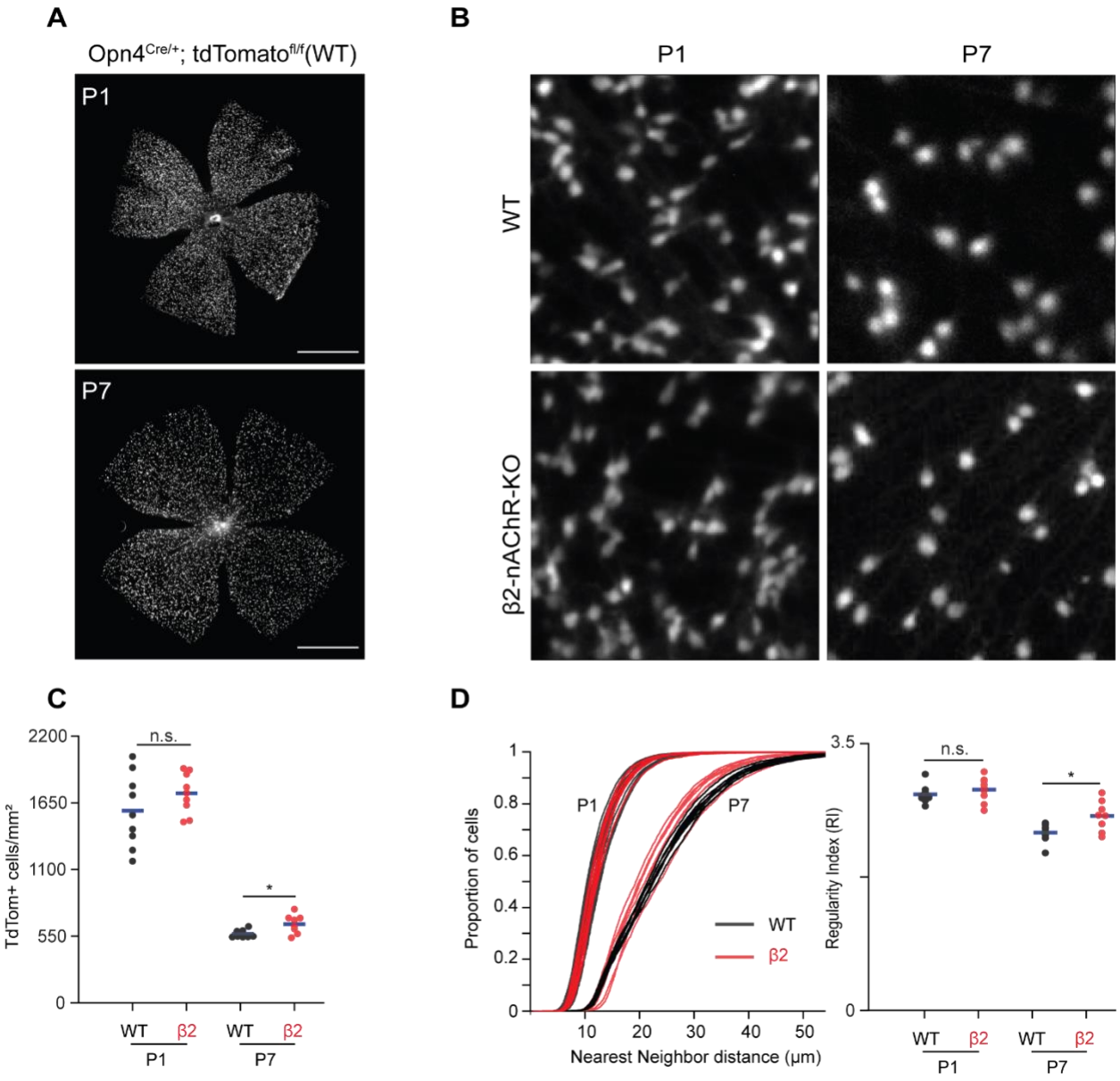

Figure 5. Stage 1 and 2 waves do not contribute to the developmental cell death of ipRGCs. **A**. Example epifluorescence images of Opn4$^{Cre/+}$; tdTomato$^{fl/fl}$ (WT) retinas at P1 and P7. Scalebars are 500 µm; each field of view is 4.7×4.7 mm. **B.** Representative 200×200 µm^2 fields of view for P1 and P7 WT and ß2-nAChR-KO retina. **C.** Average ipRGC densities across different ages and genotypes. P1 WT n=9 retinas from 6 mice, P1 ß2-nAChR-KO, 9 retinas, 7 mice; P7 WT n=8 retinas from 5 mice; P7 ß2-nAChR-KO n=8 retinas from 8 mice. p = 0.012. **D.** Cumulative distribution function of nearest neighbor distances (NND) and regularity index (mean NND/SD) from individual retinas, separated by genotype and age. p = 0.020.

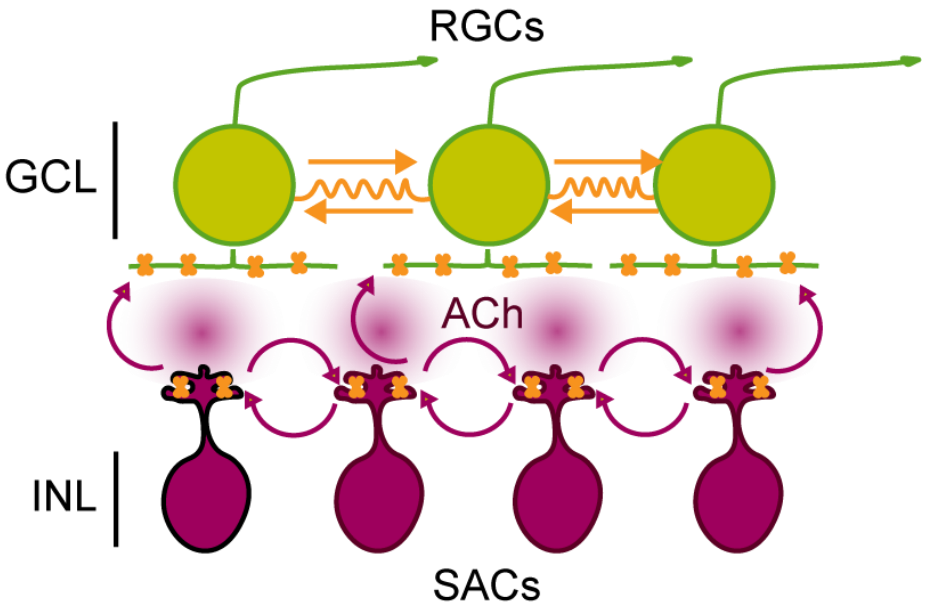

Figure 6. Schematic of Stage 1 wave initiation and propagation.

Wave initiation set by spontaneously depolarizing cholinergic amacrine cell/SAC, outlined in black, which release ACh and depolarizes neighboring cells, leading to the volumetric release of ACh. RGCs depolarized by nAChR activation (orange) via SAC-induced ACh release. Wave propagation set by RGC depolarization via gap junctional currents (orange) and volumetric ACh release.

METHODS

Animals

All animal procedures were approved by the UC Berkeley Institutional Animal Care and Use Committee and conformed to the NIH Guide for the Care and Use of Laboratory Animals, the Public Health Service Policy, and the SFN Policy on the Use of Animals in Neuroscience Research. For our calcium dye based calcium imaging, OPN4cre::tdTomato mice were generated by crossing mice B6.Cg-*Gt(ROSA)26Sor*$^{tm9(CAG\text{-}tdTomato)\ Hze}$/J mice from (Jackson Laboratory, Bar Harbor, ME) to the *Opn4*$^{Cre/+}$ reporter mouse (T. Schimdt, Northwestern University, Evanston, IL). For our GCaMP6s based calcium imaging, we generated Vglut2::GCaMP6s mice by crossing B6J.129S6(FVB)-*Slc17a6*$^{tm2(cre)Lowl}$/MwarJ mice (Jackson Laboratory, Bar Harbor, ME) to B6J.Cg-*Gt (ROSA)26Sor*$^{tm96(CAG\text{-}GCaMP6s)Hze}$/MwarJ mice (Jackson Laboratory, Bar Harbor, ME). ipRGC density measurements were conducted on P1 – P7 mice of either sex using OPN4cre::tdTomato mice.

To obtain mice that were precisely at the correct embryonic age, we set up timed pregnancies and checked vaginal plugs every morning for four days after the animals were paired. This approach led to an uncertainty of age of +/- one day. Hence we grouped data across E16-E18. Since we observed more variance within litters than across litters, we assume age was not a determining factor in our findings. We used the β2-nAChR-KO mouse line in which the β subunit of the nicotinic acetylcholine receptor is knocked out as a genetic model in which cholinergic retinal spontaneous activity is disrupted. For experiments regarding the influence of spontaneous retinal activity on the distribution of ipRGCs across the retina, we used $\beta2^{-/-}$ ::OPN4cre::tdTomato (β2-nAChR-KO) mice, generated by crossing $\beta2^{-/-}$ (A. Beaudet, Baylor University, Waco, TX) mice to OPN4cre::tdTomato mice to label all melanopsin-expressing cells. All mouse lines are maintained on a C57BL/6 genetic background. All animals used for two-photon calcium imaging experiments and immunohistochemistry were housed in 12-hour day/night cycle rooms.

Retinal preparation

On the day of the experiment, pregnant dams were deeply anesthetized via isoflurane inhalation and fetuses were harvested via a cesarean section. tdTomato positive fetuses were identified using miner goggles (Biological Laboratory Equipment Services and Maintenance Ltd., Model: GFsP-5). Fetuses were kept alive in 50 mL falcon tubes filled with oxygenated (95% O_2 5% CO_2) ACSF (in mM, 119 NaCl, 2.5 KCl, 1.3 $MgCl_2$, 1 K_2HPO_4, 26.2 $NaHCO_3$, 11 D-glucose, and 2.5 $CaCl_2$). Fetuses were then euthanized sequentially by decapitation. Eyes were immediately enucleated and retinas were dissected at room-temperature in oxygenated ACSF,

under a dissecting microscope. Isolated retinas were mounted whole over a 1–2 mm^2 hole in nitrocellulose filter paper (Millipore) with the photoreceptor layer side down and transferred to the recording chamber of a two-photon microscope for imaging. The whole-mount retinas were continuously perfused (3 ml/min) with oxygenated ACSF warmed to 32-34°C by a regulated inline heater (TC-344B, Warner Instruments) for the duration of the experiment. Additional retina pieces were kept in the dark at room temperature in ACSF bubbled with 95% O2, 5%CO2 until use (maximum 8 h).

For the calcium imaging experiments, retinas were bath loaded with the calcium indicator Cal 520 AM (AAT Bioquest) for 1-2 hours at 32°C.

Two-photon calcium imaging

Two-photon fluorescence measurements were obtained with a modified movable objective microscope (MOM) (Sutter instruments, Novator, CA) and made using an Olympus 60X, 1.00 NA, LUMPlanFLN objective (Olympus America, Melville, NY) for single cell resolution imaging (field of view, FOV: 203 x 203 um) or a Nikon 16X, 0.80 NA, N16XLWD-PF objective (Nikon, Tokyo, Japan) for large FOV (850 x 850 um) imaging. Two-photon excitation was evoked with an ultrafast pulsed laser (Chameleon Ultra II; Coherent) tuned to 920 nm to image Cal520, GCaMP6s, and tdTomato. Laser power was set between 6.5 mW-12mW for imaging of Cal520 and tdTomato expression. The microscope system was controlled by the ScanImage software (https://www.scanimage.org/). Scan parameters were [pixels/line x lines/frame (frame rate in Hz)]: [256 x 256 (1.48Hz)], at 2 ms/line. This MOM was equipped with a through-the-objective light stimulation and two detection channels for fluorescence imaging.

Epifluorescent macroscope calcium imaging

Epifluorescent calcium imaging were obtained on a custom built macroscope with an Olympus XLFLUOR4X/340 4X 0.28 NA objective, a Teledyne Kinetix camera. Collectively, this macroscope has 4.7 mm x 4.7 mm FOV, and 1.5 µm/pixel. All movies were taken at a 1 Hz frequency and pixels were binned 4 x 4 bringing the resolution down to 5.9 µm/pixel, still maintaining single cell resolution. Cal520 and GCaMP6s excitation was evoked with a 474 nm LED. A full description and building instructions can be found at: https://github.com/Llamero/DIY_Epifluorescence_Macroscope

Initiation site measurements

Macroscope recordings of Stage 1 waves were used for the manual detection of initiation sites. Small non-propagating events were identified as local regions of correlated calcium activity with

fixed areas and no wave fronts. For this analysis only, we separated waves into small and large waves to see if there were differences in initiation sites. Small propagating waves were identified as regions of correlated calcium activity with no fixed areas and with wave fronts covering up to 25% of the retina. Large propagating waves were identified as regions of correlated calcium activity with no fixed areas and with wave fronts covering up to 90% of the retina.

Pharmacology

We blocked gap junctions via application of the gap junction blocker Meclofenamic acid (MFA, 50 µM, Sigma Aldrich). We blocked the nicotinic acetylcholine signaling pathway via application of the broad nicotinic receptor antagonists hexamethonium (Hex, 100 µM, Sigma Aldrich) and epibatidine (EPB, 10 nM, Sigma Aldrich) as well as the specific antagonist dihydro-ß-erythroidine hydrobromide (DHßE, 8 µM, Sigma Aldrich).

The following procedure was used for all pharmacology experiments: We recorded baseline activity in ACSF for 8 minutes before pharmacological agents were applied to the perfusion system. We then waited 15-30 minutes for the agents to take effect before acquiring another 8-minute recording session.

Image analysis of population calcium imaging movies

Movies were preprocessed for motion correction using a MATLAB code from the Flat Iron Institute (https://github.com/flatironinstitute/NoRMCorre). The baseline movie frame (F0) was computed by taking the temporal median projection of all the movie frames. Each movie frame (F) was normalized by dividing its difference from the baseline frame (F-F0) by the baseline frame ((F-F0)/F0) to produce a ΔF/F0 movie. For movies taken on the two-photon microscope circular ROIs were drawn on all cells within the FOV. Additional circular ROIs were drawn for tdTomato+ cells. For movies taken on the macroscope a grid of 10 µm x 10 µm squares, that were spaced 1.5 pixels apart, were drawn over the whole surface of the retina using a custom FIJI macro. The ROIs and the ΔF/F0 movie were then imported into MATLAB for further analysis using custom algorithms. Traces for each FOV and ROI were computed as the mean value of the pixels enclosed by the ROI in each frame of the ΔF/F0 movie.

For transient frequency analysis, event detection was done using the findpeaks function in MATLAB, with the minimum threshold set to greater than at least 10 times the standard deviation of the baseline fluorescence, which corresponds to at least 10% $\Delta F/F_0$. The inter-transient-interval for each ROI was calculated by finding the difference between the frame of each detected transient. This difference was then converted to seconds by multiplying it to the movie's frame rate.

The area of waves was calculated for all movies taken on the macroscope. To do this, we first z-scored the percent active ROI traces and used the findpeaks function to detect individual waves, with the threshold set to a z-score of 1. After determining the time of waves, we removed any waves that occurred within the first and last 6 seconds of the movie due to them being edge cases. We then summed the number of active ROIs within 12 seconds around the wave times. This number was then divided by the total number of ROIs to get the percentage of active ROIs.

To determine if neurons participate in waves in the two-photon calcium imaging data, we employed the following bootstrapping strategy: We randomly sampled the activity of individual neurons outside of wave times a thousand times to build a baseline of neural activity. We then set a threshold of 95^{th} percentile to statistically determine if neurons exhibited a greater calcium response during a wave than at rest. We then calculated the percentage of waves each cell participated in and averaged this value for every FOV. Similarly, mean response amplitudes were calculated for each cell and then averaged for each FOV.

For a description of statistics used, please refer to the figure captions.

Analysis of ipRGC densities

To image the number of ipRGCs in fixed retinas, dissected retinas from P1 and P7 mice were fixed in 4% PFA for 30 minutes. The fixed retinas were subsequently mounted on a slide with Vectashield and a cover slip, then imaged within an hour of mounting on the macroscope. For P1 retinas, Z-stacks were acquired by manually turning the focus knob.

We first identified the centroid of each ipRGC. For P7 retinas, where there is more space between cells, we employed the following automatic segmentation. Images were bandpass filtered and somata automatically segmented using the Morpholibj (Legland et al., 2016) classic watershed tool to obtain 8-bit binarized masks. The masks were then processed in MATLAB in order to obtain the centroid locations and nearest neighbor distances for each soma. For P1 retina, where there is less space between cells and in fact cells seem to form clusters, automatic segmentation was not possible. Therefore, cells were manually marked using the ImageJ multipoint tool and soma locations exported as a CSV file. For all ages, the centroid data was imported to MATLAB for further analyses.

Density was quantified by dividing the microscope field of view up into 200×200 μm squares, manually excluding ones that did not cover the retina or covered partial or damaged parts of the retinas. Out of the resulting squares (~150 per P7 retina, ~100 per P1 retinas) 75 squares (for P7 retinas) and 50 squares (for P1 retinas) were randomly selected and the average density of TdTom+ cells in those squares calculated.

To quantify the nearest neighbor distances, we used a custom-written MATLAB code that, for each ipRGCs, identified the closest neighbor using the shortest Euclidean distance.

Statistical Tests

Details of statistical tests, number of replicates, and p values are indicated in the figures and figure captions. P values less than 0.05 were considered significant.

SUPPLEMENTARY FIGURES

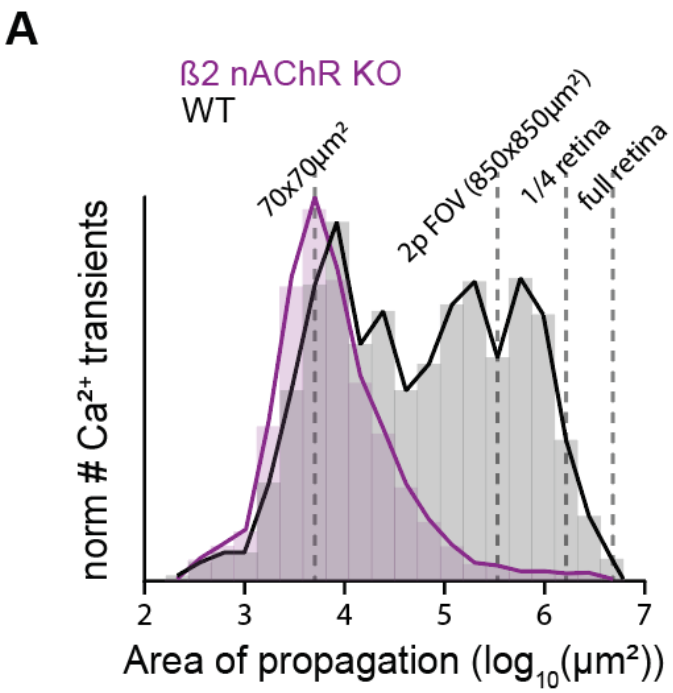

Figure 1- figure supplement 1. Distribution of Stage 1 wave sizes.

Histogram showing the distribution wave sizes for WT and B2-nAChR-KO mice. This analysis was performed using a novel algorithm that segments any activity on retinas imaged under a microscope. This algorithm can detect calcium activity as small as a few co-active neighboring cells ($\log_{10}(20x20\ \mu m^2) = 3$) to continuous waves that propagate across the entire embryonic retina ($\log_{10}(2500\ x\ 2500\ \mu m^2) = 6.8$).

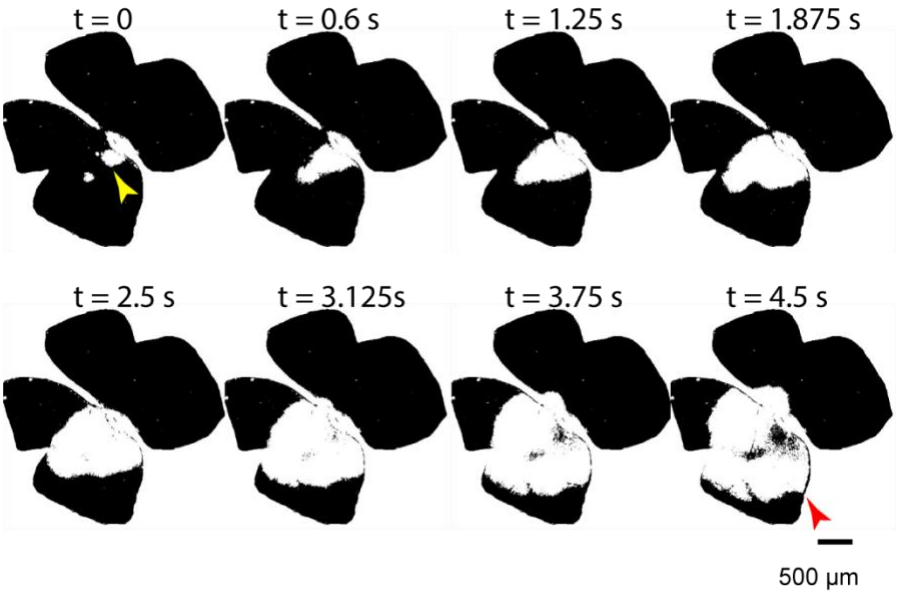

Figure 1- figure supplement 2. Average wave speed measurement.

Temporal progression of a large Stage 1 wave in WT control conditions. The average wave speed was calculated by measuring the distance between two points: the first point was marked at a random location on the edge of area defined early in the wave (yellow arrowhead; initiation spot); the second point was located at the wave edge that was parallel to the direction of propagation of the wavefront at the yellow arrowhead (red arrowhead). The speed was then calculated by dividing this distance by the propagation time of the wave.

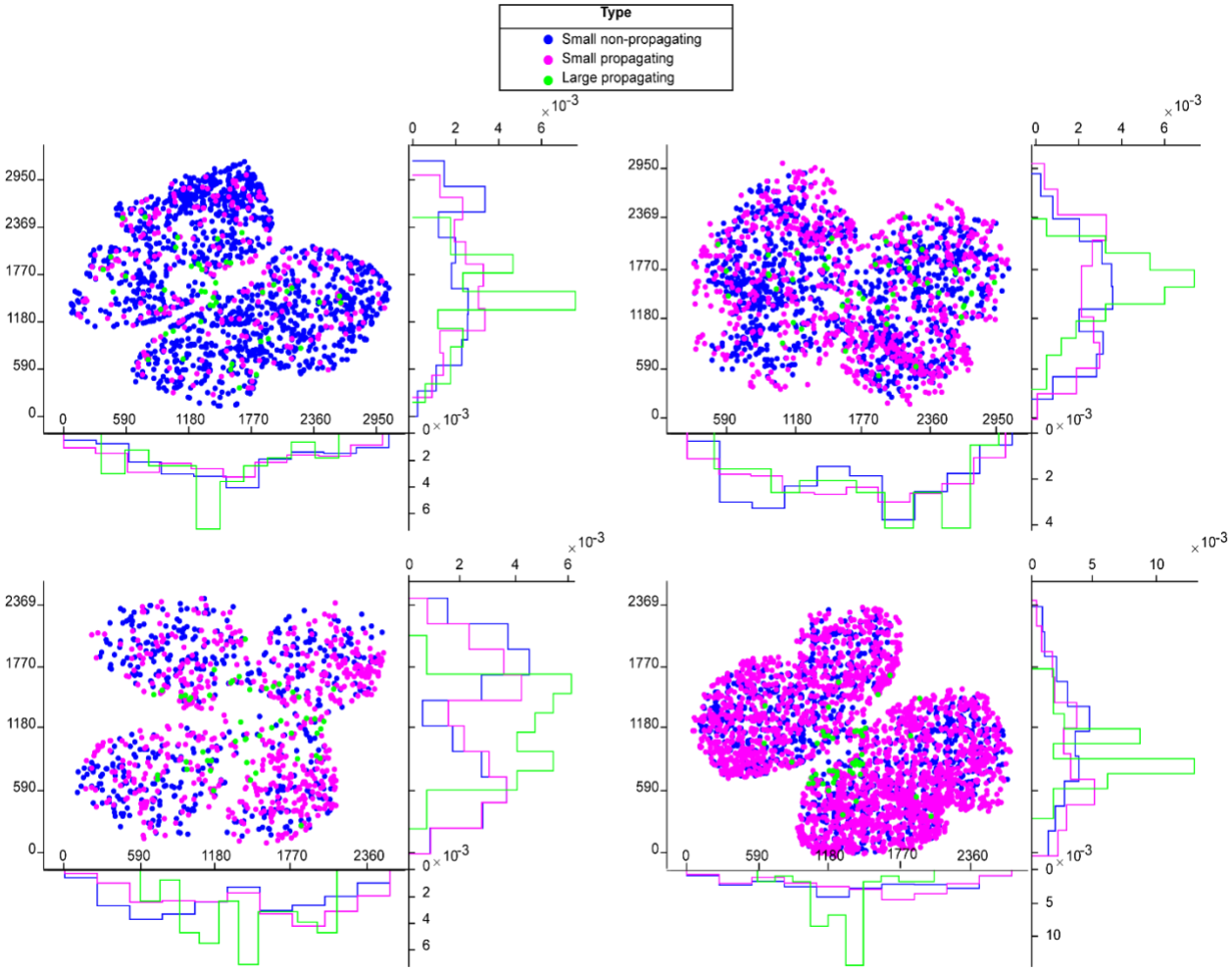

Figure 1- figure supplement 3. Distribution of Stage 1 wave initiation sites.

Scatter plots and histogram showing the distribution of initiation sites for small non-propagating events (blue), small propagating waves (magenta), and large propagating waves (green) across four E18 Vglut2cre::GCaMP6s retinas. X-axes for the scatter plots and histograms = μm. Each recording was one hour. Y-axes for scatter plots = μm. Y-axes for histograms = proportion of initiation sites.

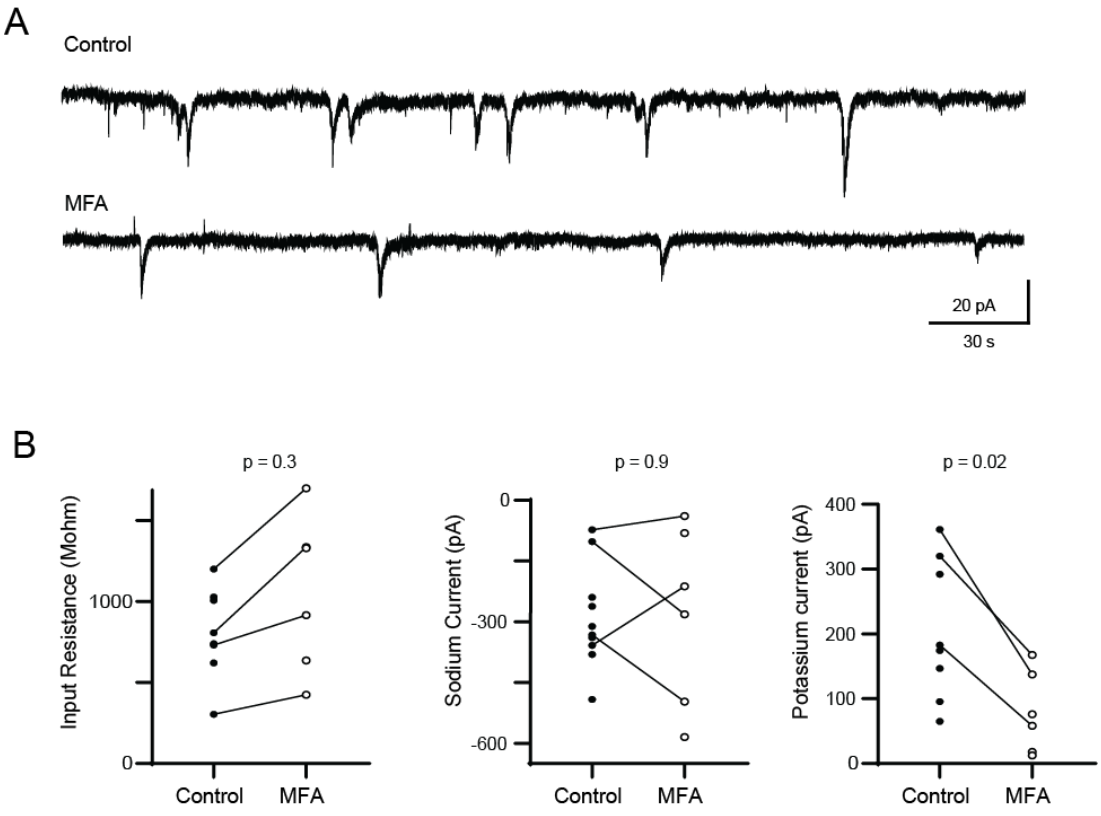

Figure 2 – Supplement 1: Controls for off-target effects of MFA on E16-E18 RGCs

A. Example voltage clamp recordings from presumptive retinal ganglion cells held at -70 mV in control solutions and after 10-20 minutes in 50 µM MFA. We observed periodic compound EPSCs that are likely representative of retinal wave in both conditions (7/7 cells in control; 5/8 cells in MFA).

B. Summary data showed the impact of bath application of MFA on input resistance (left) , voltage-gated sodium channels (middle) and potassium channels (right) activated by abrupt changes in the holding potential. The lines connect recordings that were paired – namely control and MFA application were conducted in the same cell. We observed a small increase in input resistance, consistent with a blockade of gap junctions. The variance in the voltage-gated sodium channel is consistent with the tremendous variability of ability of RGCs to fire action potentials at this young age, when different RGC types are maturing at different rates (Rothe et al., 1999). We also observed a significant reduction in the voltage-gated potassium conductance in the presence of MFA, indicating that this may be an off-target effect. As described in text, a blockade of voltage-activated K-conductances are likely to increase excitability of cells and therefore are not likely to the reason for the decrease in wave activity that we observed. Statistical significance was assessed based on unpaired t-test.

<u>Methods for voltage-clamp recordings</u>:

Whole mount retinas were held in the recording chamber by a harp and visualized using a Kohler illumination system mounted below the objective of the microscope. Presumptive RGCs were identified by their location in the immature ganglion cell layer. A hole was pierced in the inner limiting membrane of the retina using a glass recording pipette to access the RGC layer. RGCs were targeted under control of a micromanipulator (MP-225, Sutter Instruments). Recording pipettes were fabricated using a vertical puller (Narishige PC-10) and had a tip resistance of 6–7 MU. Internal solution for voltage clamp recordings was, in mM: 116 K+ D-Gluconate, 6 KCl, 2 NaCl, 20 HEPES, 0.5 EGTA, 4 ATP-Mg2+, 0.3 GTP-Na3, 10 phosphocreatine-Na2. Data were acquired using Clampex 10.2 recording software with a Multiclamp 700A amplifier (Molecular Devices) and a Digidata 1322A digitizer (Axon Instruments). Voltage clamp recordings were sampled at 10 kHz. Input resistance was computed by measuring the change in holding current in response to a -10 mV voltage change. Voltage gated sodium currents were measured as the maximum inward current evoked by step depolarizations to between -30 or -20 mV. Potassium currents were measured as the sustained current after step depolarizations to –10 mV.

Rothe T, Jüttner R, Bähring R, Grantyn R. Ion conductances related to development of repetitive firing in mouse retinal ganglion neurons in situ. J Neurobiol. 1999 Feb 5;38(2):191-206. PMID: 10022566.

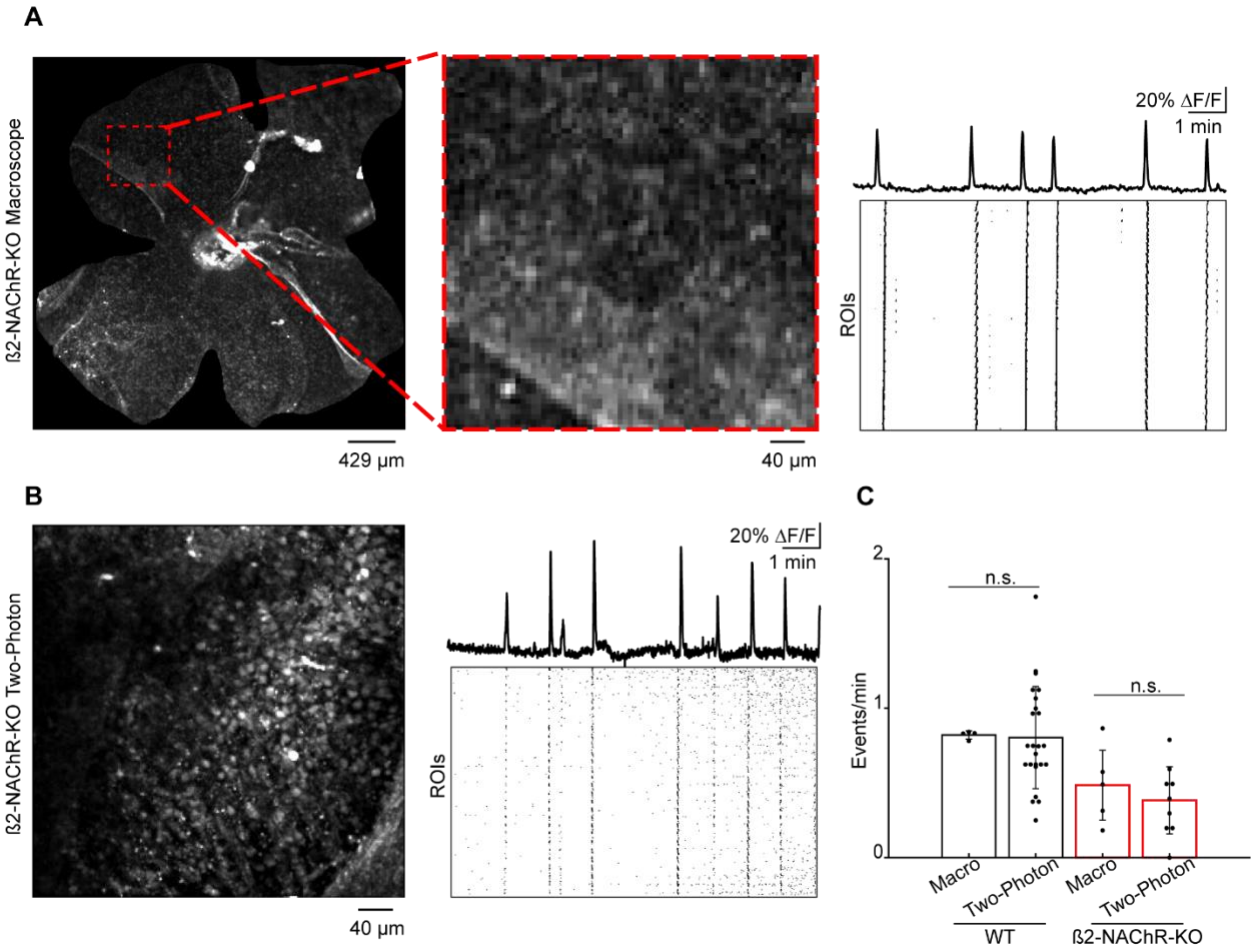

Figure 3- figure supplement 1. Frequency of Stage 1 waves in WT and β2-nAChR-KO retinas recorded on the macroscope vs the two-photon microscope.

A. *Left:* example FOV, whole mount β2-nAChR-KO, on the macroscope. Red dashed square = 425 µm^2 FOV, equivalent to two-photon FOV. *Middle:* magnified FOV. *Right:* normalized fluorescent traces showing Ca^{2+}/wave activity and raster plot summarizing Ca^{2+}/wave activity across 864 square ROIs (10 µm x 10 µm) on the macroscope. **B.** *Left:* example FOV, whole mount β2-nAChR-KO, on the two-photon microscope. *Right:* normalized fluorescent traces showing Ca^{2+}/wave activity and raster plot summarizing Ca^{2+}/wave activity across 864 square ROIs (10 µm x 10 µm) on the two-photon microscope. **C.** Bar graph showing frequency of waves on the macroscope and two-photon microscope in WT and β2-nAChR-KO. WT: n = 4 retinas (macroscope; Average ± SD: 0.82 ± 0.03), n = 24 retinas (two-photon; Average ± SD: 0.80 ± 0.34), p = 0.92. β2-nAChR-KO: n = 5 retinas (macroscope; Average ± SD: 0.48 ± 0.23), n = 9 retinas (two-photon; Average ± SD: 0.38 ± 0.22), p = 0.48.

MULTIMEDIA FILES

Link to the supplementary movies:
https://drive.google.com/drive/folders/1DsRIL0TvRL82YqZqUI125U4COp0rN0QN?usp=sharing

Video 1: Stage 1 waves
Calcium imaging of Stage 1 waves using macroscope. Total field of view is 4.7 mm x 4.7 mm. Frame rate 10 Hz. Total length of movie represents 1 minute of recording.

Video 2: Example of small non-propagating events
Calcium imaging of Stage 1 waves using macroscope. Total field of view is 4.7 mm x 4.7 mm. Frame rate 10 Hz. Total length of movie represents 15 seconds of recording. Yellow triangles depict small non-propagating events.

Video 3: Stage 1 waves in β2-nAChR-KOs
Calcium imaging of Stage 1 waves in retinas isolated from β2-nAChR-KO mice using macroscope. Total field of view is 4.7 mm x 4.7 mm. Frame rate 10 Hz. Total length of movie represents 1 minute of recording.

SOURCE DATA TABLES

Figure 1 Source Data. Inter-transient-interval, wave area, and wave speed

https://drive.google.com/drive/folders/1yk0yGzRWZ9fDARU1rvpzI_ZCPqP76zR5?usp=share_link

Figure 2 Source Data. Event frequency

Event frequency per field of view per condition (Figure 2A-D)							
ctrl	**MFA**	**ctrl**	**Hex**	**ctrl**	**EPB**	**ctrl**	**DHßE**
0.99775	0	0.873034	0.37416	0.748315	0	1.37191	0.74831
0.6236	0	0.498876	0.37416	1.122472	0	0.87303	0.62422
0.49888	0.12472	0.374157	0	0.623596	0	0.87303	0.99875
1.62135	0.24944	0.498876	0	1.746067	0.12472	0.99943	0.24986
1.24719	0.37416	0.623596	0	0.873034	0	0.8745	0
0.86333	0.24667	0.312676	0			0.62464	0.49971
0.49333	0.12333	0.187606	0				
0.98667	0.37	0.12507	0				
		0.12507	0				
		0.187606	0				
		0.997753	1.6				
		1.247191	0				
		1.184	0				

Event area and amplitude per field of view per condition (Figure 2E-H)				
mean event area			**mean event area**	
ctrl	**MFA**		**ctrl**	**DHßE**
86.900643	21.7128		96.650327	58.660131
64.162135	4.757785		93.464052	5.2287582
82.697306	73.06238		64.705882	14.542484
89.930556	15.97222		92.746914	35.227273
72.762346	13.42593		90.277778	7.9166667
52.34375	13.42593		81.448413	8.3333333
69.965278	NaN			
28.333333	NaN		**mean event amplitude**	
			5.8886222	2.3327926
mean event amplitude			1.8834566	0.8640565
1.8589475	1.584901		1.284835	0.9417388
2.1115395	1.003225		1.4888797	0.9917711
3.0430657	2.968188		0.7537867	0.4566612
1.0536635	0.708512		0.7325502	0.4633692
1.4706501	0.995778			
1.0874027	0.811886			
1.1147825	NaN			
0.8054246	NaN			

Figure 3 Source Data. Inter-transient-interval, wave area, and wave speed: WT vs b2-nAChRKO

https://drive.google.com/drive/folders/1yk0yGzRWZ9fDARU1rvpzI_ZCPqP76zR5?usp=share_link

Figure 4 Source Data. ipRGC participation and mean response amplitude

Mean wave participation and response amplitude per field of view (Figure 4C & D)					
Mean % waves cell participated			Mean response amplitude		
	RGC	ipRGCs		RGC	ipRGCs
	0.670077	0.735294		0.811785	1.004503
	0.798319	0.816631		0.610702	0.817069
	0.7249	0.727083		1.119791	1.164216
	0.816739	0.840909		1.551449	1.466176
	1	1		1.934648	2.043208
	NaN	NaN		NaN	NaN
	NaN	NaN		NaN	NaN
	0.917308	0.9125		2.664007	2.30387
	0.933333	0.902222		2.046676	2.339273
	0.851546	0.9		2.146652	2.042439
	0.799454	0.851351		1.143863	1.888502
	0.957516	0.946502		1.847363	2.218331
	0.853448	0.921875		1.257427	1.814057
	0.861667	1		1.119165	2.210363
	0.813051	0.830918		1.460548	1.539757
	0.767161	0.77551		1.16642	1.625565
	0.681853	0.781818		1.638286	1.869323
	0.739516	0.8375		1.440473	2.578029
	0.735656	0.849206		2.715635	1.592404
	0.968569	0.995169		2.415149	1.953377
	0.860558	0.881356		1.542133	1.937271
	0.866487	0.840909		1.306667	1.644891
	0.947821	0.972222		1.268351	1.804902
	0.865569	0.936782		1.151555	1.78796
	0.654217	0.711934		1.081195	1.344419
	0.756742	0.807018		1.228899	1.59941
	0.870192	0.84058		1.015366	1.336592
	0.663306	0.78481		0.82718	1.409034
	0.663725	0.822222		1.107379	1.245528

Figure 5 Source Data. Cell density analysis and regularity index

Total cell count and density per retina (Figure 5C)						
P1						
WT				**β2-NAChR-KO**		
Retina ID	**Cell Count**	**Density**		Retina ID	**Cell Count**	**Density**
OCTP1211021M1L	7317	1305.51181		BTOTP1220108M3L	6993	1768.43434
OCTP1211021M1R	7690	1367.68868		BTOTP1220124M1L	9570	1493.75
OCTP1211021M3L	8056	1300.2381		BTOTP1220124M1R	4058	1599.49495
OCTP1211021M3R	7947	1363.1068		BTOTP1220124M2L	8831	1670.73864
OCTP1220125M1R	8445	1686.74699		BTOTP1220124M3L	8572	1676.63044
OCTP1220125M2R	10609	1866.99029		BTOTP1220209M2R	7630	1361.43617
OCTP1220125M3L	10930	1986.05263		BTOTP1220209M3R	8720	1555.58252
OCTP1220125M4L	9265	1602.45098		BTOTP1220209M4L	8521	1903.01339
OCTP1220125M4R	9633	1843.5		BTOTP1220209M4R	10279	1850.93458
Average		**1591.36514**				**1653.335**
Std		**267.661197**				**172.700938**
P7						
	Cell Count	**Density**			**Cell Count**	**Density**
OCTP1220222M1R	5227	555.789474		BTOTP1211004M1R	4874	660.912698
OCTP1220222M2L	5466	561.82266		BTOTP1211004M2L	6366	716.715976
OCTP1220222M3L	5414	536.162791		BTOTP1211004M2R	6079	796.25
OCTP1220222M4R	5457	594.221106		BTOTP1220222M1R	6345	768.125
OCTP1220222M5R	5428	628.106509		BTOTP1220222M2L	6342	569.186047
OCTP1220222M6L	5487	593.88587		BTOTP1220222M2R	5053	534.947644
OCTP1220222M7L	5924	597.60101		BTOTP1220222M3L	5965	653.314917
OCTP1220222M8R	5645	551.064886		BTOTP1220222M3R	6035	723.45679
Average		**577.331788**				**677.863634**
Std		**30.7934156**				**91.7110822**

Nearest neighbor distance and Regularity index (RI) (Figure 5D)									
P1									
WT					**β2-NAChR-KO**				
Retina ID	**Mean**	**SD**	**Median**	**RI**	**Retina ID**	**Mean**	**SD**	**Median**	**RI**
OCTP1211021M1L	13.64	4.712	12.588	2.9	BTOTP1220108M3L	12.56	4.18	11.7806	3.01
OCTP1211021M1R	13.7	4.421	12.8529	3.1	BTOTP1220124M1L	12.19	4.22	11.3118	2.89
OCTP1211021M3L	13.56	4.924	12.5658	2.75	BTOTP1220124M1R	13.3	5.07	12.2187	2.62
OCTP1211021M3R	13.02	4.673	11.9694	2.79	BTOTP1220124M2L	12.43	4.41	11.5082	2.82
OCTP1220125M1R	12.05	4.278	11.0771	2.82	BTOTP1220124M3L	11.79	4.36	10.839	2.7
OCTP1220125M2R	11.48	4.095	10.5976	2.8	BTOTP1220209M2R	12.98	4.14	12.2119	3.13
OCTP1220125M3L	11.23	3.933	10.3803	2.86	BTOTP1220209M3R	12.87	4.26	12.0152	3.02
OCTP1220125M4L	12.29	4.404	11.4055	2.79	BTOTP1220209M4L	11.74	4.02	10.8714	2.92
OCTP1220125M4R	11.72	4.373	10.8617	2.68	BTOTP1220209M4R	11.88	4.01	11.0633	2.96
Average	**12.52**	**4.424**	**11.5887**	**2.83**		**12.41**	**4.3**	**11.5356**	**2.9**
Std	**0.976**	**0.31**	**0.93293**	**0.12**		**0.561**	**0.32**	**0.54936**	**0.16**
P7									
Retina ID	**Mean**	**SD**	**Median**	**RI**	**Retina ID**	**Mean**	**SD**	**Median**	**RI**
OCTP1220222M1R	24.35	9.989	22.4473	2.44	BTOTP1211004M1R	23.29	8.16	21.4777	2.86
OCTP1220222M2L	23.98	9.753	22.4406	2.46	BTOTP1211004M2L	21.8	7.93	20.117	2.75
OCTP1220222M3L	25.03	12.12	23.3751	2.07	BTOTP1211004M2R	21.01	7.97	19.3436	2.64
OCTP1220222M4R	24.08	10.65	22.3262	2.26	BTOTP1220222M1R	21.61	8.44	19.913	2.56
OCTP1220222M5R	23	9.807	21.4488	2.35	BTOTP1220222M2L	23.82	10.2	21.8928	2.33
OCTP1220222M6L	23.62	9.888	21.9383	2.39	BTOTP1220222M2R	25.62	11.3	23.7144	2.28
OCTP1220222M7L	23.46	9.788	21.9111	2.4	BTOTP1220222M3L	22.71	9.28	21.0318	2.45
OCTP1220222M8R	24.46	10.63	22.6454	2.3	BTOTP1220222M3R	21.82	8.54	20.2045	2.55
Average	**24**	**10.33**	**22.3166**	**2.33**		**22.71**	**8.97**	**20.9619**	**2.55**
Std	**0.637**	**0.81**	**0.57591**	**0.13**		**1.501**	**1.2**	**1.40002**	**0.2**

KEY RESOURCES TABLE

Reagent type (species) or resource	**Designation**	**Source or reference**	**Identifiers**	**Additional information**
Strain, strain background (*Mus musculus*; male & female)	C57BL/6J (wild type)	The Jackson Laboratory	strain: 000664	Background strain used for mouse crosses
Strain, strain background (*Mus musculus*; male & female)	B6.Cg-*Gt(ROSA)26Sor*$^{tm9(CAG-tdTomato)\ Hze}$/J	The Jackson Laboratory	strain: 012586	Used to express tdTomato in ipRGCs
Strain, strain background (*Mus musculus*; male & female)	B6J.129S6(FVB)-*Slc17a6*$^{tm2(cre)Lowl}$/MwarJ mice	The Jackson Laboratory	strain: 007676	Used to drive expression of GCaMP6s in retinal ganglion cells
Strain, strain background (*Mus musculus*; male & female)	B6J.Cg-*Gt(ROSA)26Sor*$^{tm96(CAG-GCaMP6s)Hze}$/MwarJ	The Jackson Laboratory	strain: 028866	Used to measure calcium dynamics in retinal ganglion cells
Strain, strain background (*Mus musculus*; male & female)	Opn4$^{cre/+}$	Ecker et al., *Neuron*, 2010. doi: 10.1016/j.neuron.2010.05.023. PMID: 20624591; PMCID: PMC2904318.		Used to drive expression of tdTomato in ipRGCs

Strain, strain background (*Mus musculus*; male & female)	β2-nAChR-KO	Bansal et al., *J Neurosci*, 2000. doi: https://doi.org/10.1523/JNEUROSCI.20-20-07672.2000		Targeted deletion generated by Xu et al. (*J Neurosci*, 1999) and maintained in our lab since

Chemical compound, drug	Meclofenamic acid	Sigma-Aldrich	M4531	Gap junction blocker
Chemical compound, drug	Hexamethonium	Sigma-Aldrich	H0879	Non-α7 nAChR antagonist
Chemical compound, drug	Epibatidine	Sigma-Aldrich	E1145	General nAChR desensitizing agonist
Chemical compound, drug	Dihydro-ß-erythroidine hydrobromide	Sigma-Aldrich	D149	α4 and β2 containing nAChR antagonist
Software, algorithm	ScanImage	Vidrio Technologies, LLC	RRID:SCR_014307	2-photon image acquisition software
Software, algorithm	FIJI/ImageJ	Created at National Institutes of Health; Schindelin et al., *Nature Methods*, 2012.	RRID:SCR_002285	Used for image processing and analysis

		doi:10.1038/nmeth.2019		
Software, algorithm	MATLAB	MathWorks	RRID:SCR_001622	Custom scripts used for data processing, analysis

Software, algorithm	NormCorre: Non-Rigid Motion Correction	Flatiron Institute, Simons Foundation; Pnevmatikakis and Giovannucci, *J Neurosci Methods*, 2017. doi: https://doi.org/10.1016/j.jneumeth.2017.07.031		For 2D registration of calcium imaging movies
Software, algorithm	Micro-Manager 2.0	Edelstein et al., *J. Biol. Methods*, 2014. https://doi:10.14440/jbm.2014.36	RRID:SCR_000415	Macroscope image acquisition software
Software, algorithm	PyCharm: LED driver GUI code	Four_Channel_MHz_LED_Driver/Software/GUI_code at master · Llamero/Four_Channel_MHz_LED_Driver · GitHub		GUI code to control LED driver for macroscope imaging

Chapter 3

Conclusions and Future Directions

Understanding the circuit mechanisms underlying the spatiotemporal features of Stage 1 waves

The cellular mechanisms governing the initiation and propagation of Stage 2 and 3 waves have been extensively studied. Although progress has been made in understanding those that govern Stage 1 waves much work remains to be done. The results from my thesis work reveal the mechanisms that mediate the spatiotemporal properties of Stage 1 waves. Specifically, we show that both cholinergic signaling and gap junctions are important for the generation of Stage 1 waves (**Chapter 2, Figure 2 & 3**). However, we still do not know exactly how SACs are releasing acetylcholine at this age and which set of nAChRs are important for initiation and propagation. Additionally, it is unclear if gap junctions are needed for both initiation and propagation. Although my data would suggest they are important for both (**Chapter 2, Figure 2**), a mechanism by which gap junctions could contribute to wave initiation remains to be tested.

Acetylcholine signaling is important for the initiation and propagation of Stage 1 waves, but little is known about its release mechanism in embryonic retinas or the exact contribution of different nAChR subtypes in wave propagation. A unique characteristic of Stage 1 waves is its broad distribution of wave areas, which seem to depend on the type of nAChRs available. My data has shown that removing β2 expressing nAChRs, either genetically or via the application of DHßE to target the α4β2 nAChRs, dramatically reduces the area of wave propagation, but did not abolish waves (**Chapter 2, Figure 2 & 3**). Waves were only abolished when all nAChRs were blocked with Hex in WT retinas or when gap junctions were blocked in β2-nAChRs-KOs (**Chapter 2, Figure 2 & 3**). This suggests that an array of nAChRs is expressed by RGCs and SACs embryonically and are important for setting up this broad distribution of wave areas. Embryonically, both RGCs and SACs express nAChRs with combination of α3 & α4 and β2 & β4 subunits, with RGCs also expressing the β3 subunits (Peng et al., 2019; Shekhar et al., 2022). Both the α3 & α4 subunits can form functional nAChRs with both the β2 & β4 subunits (Xu et al., 1999), and α3β2 as well as α4β2 nAChRs are present in the developing mouse retina (Bansal et al., 2000). Previous work looking at the role of the α3 subunit in the generation of Stage 2 waves and found that by knocking out this subunit, you can alter the spatiotemporal properties of these waves, making them more like Stage 1 waves (Bansal et al., 2000). Additionally, they found that knocking out the β2 subunit significantly reduced the frequency of Stage 2 waves, and that knocking out both the β2 & β4 gave them the same results observed in the β2 single KO (Bansal et al., 2000). This determined that unlike the β2 subunit, the β4 subunit is not important for the generation of Stage 2 waves. Future experiments looking at the effects of genetically knocking out additional subunits will improve our understanding of which types of nAChRs are important for either initiation or propagation. Lastly, Stage 2 waves propagate through a cholinergic network between neighboring SACs (Ford et al., 2012). To know if a similar

network exists in the embryonic retina, two-photon calcium imaging of SACs and electrophysiological recordings during Stage 1 waves will be crucial.

Gap junctions have been implicated in the generation and regulation of retinal waves and this is especially true for stage 1 waves, however little is known about the mechanism by which they are involved in wave initiation and propagation (Kirkby et al., 2013; Syed et al., 2004). Although I show that gap junctions are important for both wave initiation and propagation of Stage 1 waves (**Chapter 2, Figure 2**), exactly how this happens remains to be determined. A gap junction mediated initiation model for Stage 1 waves has been deduced, where events are initiated by RGCs undergoing rare and random depolarizations that propagate entirely via electrical synapses (Kähne et al., 2019). Supporting this model is the observation of random, but frequent depolarization of RGCs between waves and after waves are blocked. Furthermore, an analysis of wave initiation sites showed a random distribution across the retina which is in line with the random depolarization of RGCs. To determine if the depolarization of a single RGC is sufficient for wave initiation current injections to a single RGCs, in tandem with calcium imaging, as was done with SACs to determine the initiation mechanism of Stage 2 waves (Ford et al., 2012).

Using connexin (Cx) knockout (KO) mice would provide us with a deeper understanding of the role gap junctions play in the initiation and propagation of Stage 1 waves. Previous work investigating the role of gap junctions in the generation of Stage 2 waves looked at changes in their spatiotemporal properties in Cx36 and 45 KOs. They found that Cx36 and 45 KO mice had relatively normal Stage 2 and 3 waves (Blankenship et al., 2011). The main effects observed were an increase in the number of action potentials between wave events and an increase in wave frequency (Blankenship et al., 2011). Additionally, eye specific segregation in the dorsal lateral geniculate nucleus was significantly reduced in Cx36 and Cx45 double knockouts (Blankenship et al., 2011), indicating this small disruption in spatiotemporal properties were sufficient to alter this important development step. Investigating the effects of these Cx knockouts on the spatiotemporal properties of Stage 1 waves would be beneficial for understanding how the contribute to Stage 1 wave generation.

Elucidating the role of stage 1 waves in visual system development

Stage 1 waves occur during a period of retinal development when cells are undergoing proliferation, differentiation, migration, and death (Lucas & Schmidt, 2019; McNeill et al., 2011; Farah & Easter, 2005; Bahr, 2000), yet the role they play in regulating these processes has yet to be investigated. During the propagation of retinal waves, RGCs experience a significant influx of calcium (Ca^{2+}), as indicated by our ability to observe them with calcium imaging. This influx of Ca^{2+} occurs throughout the length of the cell, from the some to the axon terminals. Since cholinergic signaling is important for the initiation and propagation of Stage 1 waves, the Ca^{2+} influx observed at the soma is likely due to the increased permeability of nAChRs to Ca^{2+} upon the binding of acetylcholine (Shen & Yakel, 2009). An influx of Ca^{2+} at the soma can trigger a multitude of gene expression pathways important for cell proliferation, differentiation, migration, and death (Gu & Spitzer, 1995; Toth et al., 2016), all of which occur during Stage 1 waves.

Although we did not see a change in ipRGC density or spatial distribution in the β2-nAChR-KO (**Chapter 2, Figure 5**), it is possible that the remaining activity in the KO was sufficient to sustain normal ipRGC development. If a Stage 1 wave deficient mouse model can be generated, it would be interesting to see if the proliferation, differentiation, migration, and death of ipRGCs is unchanged.

RGC axonal growth and guidance is a process that occurs postnatally, but ipRGCs begin this process embryonically and little is known about the mechanisms regulating it. Postnatal axonal growth and guidance in the developing visual system occurs via growth cones, axon guidance molecules and retinal waves (Simon et al., 1994; McLaughlin & O'Leary, 2005; Feldeim & O'Leary, 2010). Gradients of axon guidance molecules ephrinA and ephrinB along with their receptors EphA and EphB are important for setting up the anterior-posterior and medial-lateral topographic organization of RGC axon terminal, respectively (McLaughlin & O'Leary, 2005; Feldheim & O'Leary, 2010). However, ipRGCs send their axons to the brain as early as E17, when their axons are found at the optic chiasm, right below the SCN (McNeill et al., 2011). The innervation of the suprachiasmatic nucleus (SCN) occurs soon after birth, with some axons projecting into the SCN as soon as P0 (McNeill, 2011). Although ipRGC axons arrive at the chiasm during embryonic development, SCN innervation does not start until postnatal development, when the ephrin gradients and Stage 2 waves present in the SC have been shown to be important for the refinement of the axon terminals and retinotopic maps (Tiriac et al., 2018; Kirkby et al., 2013; Dhande et al., 2011; McLaughlin et al., 2003). Recent work has shown that blocking neural activity in SCN projecting RGCs in P1 retinas, inhibits the refinement of axon terminals in the SCN (Negueruela, et al., 2022). This suggests that spontaneous activity is important for the refinement of axon terminals in the SCN. Our studies provide strategies for loss of function studies that test a role for Stage 1 waves in RGC innervation to multiple targets in the brain.

REFERENCES

Bahr, M. (2000). Live or let die - retinal ganglion cell death and survival during development and in the lesioned adult CNS. *Trends in Neurosciences*, *23*(10), 483–490. https://doi.org/10.1016/S0166-2236(00)01637-4

Bansal, A., Singer, J. H., Hwang, B. J., Xu, W., Beaudet, A., & Feller, M. B. (2000). Mice Lacking Specific Nicotinic Acetylcholine Receptor Subunits Exhibit Dramatically Altered Spontaneous Activity Patterns and Reveal a Limited Role for Retinal Waves in Forming ON and OFF Circuits in the Inner Retina. *Journal of Neuroscience*, *20*(20), 7672–7681. https://www.jneurosci.org/content/20/20/7672.long

Blankenship, A. G., Hamby, A. M., Firl, A., Vyas, S., Maxeiner, S., Willecke, K., & Feller, M. B. (2011). *The Role of Neuronal Connexins 36 and 45 in Shaping Spontaneous Firing Patterns in the Developing Retina*. *31*(27), 9998–10008. https://doi.org/10.1523/JNEUROSCI.5640-10.2011

Dhande, O. S., Hua, E. W., Guh, E., Yeh, J., Bhatt, S., Zhang, Y., Ruthazer, E. S., Feller, M. B., & Crair, M. C. (2011). Development of Single Retinofugal Axon Arbors in Normal and 2 Knock-Out Mice. *Journal of Neuroscience*, *31*(9), 3384–3399. https://doi.org/10.1523/jneurosci.4899-10.2011

Farah, M. H., & Easter, S. S. (2005). Cell birth and death in the mouse retinal ganglion cell layer. *Journal of Comparative Neurology*, *489*(1), 120–134. https://doi.org/10.1002/cne.20615

Feldheim, D., & O' Leary, D. (2010). Visual Map Development: Bidirectional Signaling, Bifunctional Guidance Molecules, and Competition. *Cold Spring Harb Perspect Biol*. 10.1101/cshperspect.a001768

Ford, K. J., Félix, A. L., & Feller, M. B. (2012). *Cellular Mechanisms Underlying Spatiotemporal Features of Cholinergic Retinal Waves*. https://doi.org/10.1523/JNEUROSCI.5309-12.2012

Gu, X., & Spitzer, N. C. (1995). Distinct aspects of neuronal differentiation encoded by frequency of calcium transients. *Nature*, *375*(June), 784–787.

Kähne, M., Rüdiger, S., Kihara, A. H., & Lindner, B. (2019). Gap junctions set the speed and nucleation rate of stage I retinal waves. *PLoS Computational Biology*, *15*(4), 1–15. https://doi.org/10.1371/journal.pcbi.1006355

Kirkby, L. A., Sack, G. S., Firl, A., & Feller, M. B. (2013). A role for correlated spontaneous activity in the assembly of neural circuits. *Neuron*, *80*(5), 1129–1144. https://doi.org/10.1016/j.neuron.2013.10.030

Lucas, J. A., & Schmidt, T. M. (2019). Cellular properties of intrinsically photosensitive retinal ganglion cells during postnatal development. *Neural Development*, *14*(1), 1–19. https://doi.org/10.1186/s13064-019-0132-2

McLaughlin, T., Torborg, C. L., Feller, M. B., & O'Leary, D. D. M. (2003). Retinotopic map refinement requires spontaneous retinal waves during a brief critical period of development. *Neuron*, *40*(6), 1147–1160. https://doi.org/10.1016/S0896-6273(03)00790-6

McLaughlin, T., & O'Leary, D. D. M. (2005). Molecular gradients and development of retinotopic maps. *Annual Review of Neuroscience*, *28*, 327–355. https://doi.org/10.1146/annurev.neuro.28.061604.135714

McNeill, D. S., Sheely, C. J., Ecker, J. L., Badea, T. C., Morhardt, D., Guido, W., & Hattar, S. (2011). Development of melanopsin-based irradiance detecting circuitry. *Neural Development*, *6*(1), 2–11. https://doi.org/10.1186/1749-8104-6-8

Negueruela, S., Morenilla, C., Herrera, M., Coca, Y., Florez-Paz, D., López-Cascales, M. T., . . . Herrera, E. (2022). Perinatal correlated retinal activity is required for the wiring of visual axons in non-image forming nuclei. *bioRxiv*. 2022.07.27.501692. https://doi.org/10.1101/2022.07.27.501692

Peng, Y.-R., Shekhar, K., Yan, W., Herrmann, D., Sappington, A., Bryman, G. S., . . . Sanes, J. R. (2019). Molecular Classification and Comparative Taxonomics of Foveal and Peripheral Cells in Primate Retina. *Cell*, 1222-1237.e22. https://doi.org/10.1016/j.cell.2019.01.004.

Shekhar, K., Whitney, I. E., Butrus, S., Peng, Y.-R., & Sanes, J. R. (2022). Diversification of multipotential postmitotic mouse retinal ganglion cell precursors into discrete types. *ELife*, *11*. https://doi.org/10.7554/eLife.73809

Shen, J. X., & Yakel, J. L. (2009). Nicotinic acetylcholine receptor-mediated calcium signaling in the nervous system. *Acta Pharmacologica Sinica*, *30*(6), 673–680. https://doi.org/10.1038/aps.2009.64

Simon, D. K., Roskies, A. L., & O'Leary, D. D. M. (1994). Plasticity in the development of topographic order in the mammalian retinocollicular projection. *Developmental Biology*, *162*(2), 384–393. https://doi.org/10.1006/dbio.1994.1095

Steinhardt, P. J., Jeong, H., Saitoh, K., Tanaka, M., Abe, E., Tsai, A. P., Gomez, T. M., Spitzer, N. C., Wilson, S. B., Kent, S. C., Patton, K. T., Orban, T., Jackson, R. A., Exley, M., Porcelli, S., Schatz, D. A., Atkinson, M. A., Balk, S. P., Strominger, J. L., … Rance, S. J. (1999). letters to nature corrections Experimental veri ® cation of the quasi-unit-cell model of quasicrystal structure In vivo regulation of axon extension and path ® nding by growth-cone calcium transients Extreme Th1 bias of invariant Va24JaQ Tcells in type 1 . *Nature*,

399(May).

Syed, M. M., Lee, S., Zheng, J., & Zhou, Z. J. (2004). Stage-dependent dynamics and modulation of spontaneous waves in the developing rabbit retina. *Journal of Physiology*, *560*(2), 533–549. https://doi.org/10.1113/jphysiol.2004.066597

Tiriac, A., Smith, B. E., & Feller, M. B. (2018). Light Prior to Eye Opening Promotes Retinal Waves and Eye-Specific Segregation. *Neuron*, *100*(5), 1059-1065.e4. https://doi.org/10.1016/J.NEURON.2018.10.011

Toth, A. B., Shum, A. K., & Prakriya, M. (2016). Regulation of neurogenesis by calcium signaling. *Cell Calcium*, *59*(2–3), 124–134. https://doi.org/10.1016/j.ceca.2016.02.011

Xu, W., Orr-Urtreger, A., Nigro, F., Gelber, S., Sutcliffe, C. B., Armstrong, D., Patrick, J. W., Role, L. W., Beaudet, A. L., & De Biasi, M. (1999). Multiorgan autonomic dysfunction in mice lacking the β2 and the β4 subunits of neuronal nicotinic acetylcholine receptors. *Journal of Neuroscience*, *19*(21), 9298–9305. https://doi.org/10.1523/jneurosci.19-21-09298.1999